Corrosion behavior of WC-Co coatings deposited by Cold Gas Spray onto AA 7075-T6

F. S. da Silva[a,b], N. Cinca[b], S. Dosta[b], I. G. Cano[b], M. Couto[b], J. M. Guilemany[b], A. V. Benedetti[a *]

[a]*São Paulo State University (Unesp), Institute of Chemistry, Araraquara, Rua Prof. Francisco Degni, 55, P.O. Box 355, 14800-060- Araraquara, SP, Brazil.*

[b]*Barcelona University, CPT, Martí I Franqués 1, 08028 Barcelona, Spain.*

*Corresponding author

E-mail address: benedeti@iq.unesp.br (A.V. Benedetti)

Abstract

In this work the morphology, chemical, mechanical and corrosion characterization of WC-12Co and WC-25Co coatings prepared by Cold Gas Spray (CGS) onto AA 7075-T6 alloy was studied. The cross section images of coatings showed a dense structure, with low porosity. The coating thickness was 65 µm for WC-12Co and 118 µm for WC-25Co. XRD showed that coatings are almost oxide free and no fragile phases were formed. SEM images and electrochemical results after ~700 h showed that WC-25Co is better than WC-12Co for anti-corrosion purpose. WC-12Co and WC-25Co coatings withstood, respectively, 1000 and 3000 h of salt fog spray test.

Keywords: cold spray, metal coatings, EIS, polarization, SEM, XRD.

1. Introduction

Aluminum alloys such as AA 7075-T6 are widely used in aircraft manufacture as well as in many other industries as structural components due to their high-strength/weight ratio [1,2]. Nevertheless, those alloys can be affected by different forms of corrosion such as pitting and galvanic corrosion, intergranular corrosion, stress corrosion cracking or exfoliation corrosion [1–5].

It is well known that in chloride ion containing solution AA 7075-T6 alloy are susceptible mainly to severe localized corrosion and intergranular corrosion due the presence of elements like Mg, Zn, Cu and others [1,2,6]. Localized corrosion usually sets in at heterogeneities in the microstructure of the alloy, such as coarse intermetallic phases, constituent particles, inclusions or even precipitates or segregations at grain boundaries. Among these, coarse intermetallic phases always attracted attention as they are the most prominent initiation sites in alloys due to galvanic coupling effects. It is well known that Cu containing intermetallic phases are cathodic with respect to the matrix and thus promote the dissolution of the surrounding matrix [6]. The Mg or Zn rich intermetallic are usually anodic with respect to the matrix and hence dissolve first. The localized corrosion can lead to sudden and unpredicted failures and deterioration of metal structures increasing the costs and maintenance. To protect Al alloys from localized and other forms of corrosion and to improve the wear resistance protective WC-Co coatings have been used [7-12].

WC-Co coatings are composed of WC particles dispersed in Co metal matrix [7,9-13]. This coating has the high temperature and abrasion resistance of ceramics and the ductility of metallic materials. Due to these properties, WC-Co coatings are widely used for applications when high mechanical performance and corrosion resistance are required, as example, turbine blades of the hydro power plants, aeroplane landing gear, diesel engines and rollers in paper industries [13-15].

WC-Co materials were applied as coatings by High-Velocity Oxy-Fuel (HVOF) on steel [16-26] and aluminum alloys [7,8], high velocity air-fuel (HVAF) [27], plasma spraying [27-30], low pressure plasma spray [27] and electrospark granules [31]. These materials have been employed for different purposes when high abrasion, sliding, fretting and erosion resistances are required, and these properties depend on the density and particle size of the powder, spraying conditions and spray technique used [7,12,15,32]. Lately, these coatings have been mainly used to obtain material with low decarburization [22], to improve the surface hardness [22,33], without developing brittle phases [34], to increase adhesion of the coating/substrate by thermal treatment or adding a layer of different material on the substrate [30], to act as a barrier to avoid attack of a liquid metal to the substrate [34], to protect steel from water droplet erosion [35], to increase the wear resistance at temperatures up to 600 ^{o}C in air, not in argon atmosphere or higher temperatures [27 36].

These techniques use high temperatures during spray which can reach up to 3000 °C, leading to total or partial melting of the particles and then they are accelerated by a compressed gas flow to the surface [7,12]. The problems of the HVOF coatings are intrinsic characteristics of the process which lead to the formation of pores, cracks and chemical modification of the feedstock powder [7,12]. Cracks and residual stress mainly occur between the layers of deposited material, due to the fast solidification of sprayed particles, leading to the formation of a porous coating that allow the diffusion of electrolyte to the substrate, causing the corrosion to be initiated. The use of high temperatures leads to changes in the phases of the feedstock material due to the material degradation and the formation of oxides and brittle phases, which can change the mechanical properties and corrosion resistance of coatings [13,7,12,37-39].

When WC-Co is deposited onto aluminum alloys using HVOF, the formation of the coating can be difficult because of the difference in the thermal expansion coefficient between

the coating and substrate [7]. This difference leads to a residual stress which affects the mechanical stability of the coating and its corrosion performance. For these substrates, the contraction during cooling causes stresses and cracks formation not only between layers, but also on the substrate/coating interface resulting in coating delamination [7]. To overcome this problem, the use of a substrate cooling system or resins applied to substrate surface before deposition were suggested [40-42]. The use of post-treatment or coatings sealing have been also investigated [43], however, these make the process more expensive and slower. On the other hand, the Cold Gas Spray (CGS) technology have been able to produce thicker, wear and corrosion resistance WC-Co coatings with lower cost [9-12,44,45] when applied on steel [9,45], and aluminum alloys [9-11]. In CGS a solid powder is heated at low temperatures (<1000 °C) and the particles accelerated between 500 and 1200 m/s [9,11,45,46], depending on the gas used, spraying parameters and nozzle design.

When the velocity of the particles exceeds certain critical value, as to reach the substrate in CGS technology, the impact energy of the particle on the substrate causes an intense plastic deformation of the particle and substrate [47]. This energy makes the material to be semi-molten, which is rapidly cooled, generating the splats and interconnected particles resulting in coating formation [46]. Differently from HVOF, the high kinetic and low thermal energy in the CGS technology achieved during the spraying process [48] diminish residual stresses, oxidation, and degradation of feedstock material [46,49]. Therefore, these characteristics guarantee that CGS can produce coatings using metallic-ceramic starting materials. Some studies have been investigated the production of cobalt-based coatings by CGS in different conditions such as spray to various substrates, feedstock powder of different particle sizes, composition and morphology and different spray parameters [10-12,45,50].

The evaluation of coatings sprayed using feedstock WC-Co powders with different Co content onto different substrates was also investigated [11,12,50]. Coatings formed from

powders with higher amount of Co showed higher deposition efficiency and denser microstructure, since a larger binder content leads to greater plastic deformation of the particles and high effectiveness in interlocking between particles and particle/substrate.

The influence of spraying parameters and particle size (nano and micrometer) were investigated on the deposition of WC-Co coatings on stainless steel [45]. The obtained coatings from the nanometric powder and at optimized conditions showed hardness of 2053 HV and thicknesses up to 900 µm, and when micrometer particles were used, the hardness decreased to 918 HV and thickness to 200 µm [45].

Couto et al. [10,12] have evaluated the microstructure and mechanical properties of WC-Co coatings obtained by HVOF and CGS onto AA 7075-T6 alloy. The WC-25Co coatings obtained from both techniques showed a dense microstructure and thickness of 211 µm (CGS) and 163 µm (HVOF). CGS coatings adhesion (65 ± 4) MPa was almost three times greater than the HVOF while the hardness of both coatings was ≈ 900 HV. XRD analysis of the starting material and coatings showed brittle phases such as W_2C, W, Co_6W_6C and Co_3W_3C when deposited by HVOF. On the other hand, no change of the starting materials was observed to CGS coatings. For the two coatings, the abrasive wear rate was $\approx 2\times10^{-5}$ mm^3/Nm, and the sliding wear test showed that HVOF coating lost five times more material than the CGS one.

In the present work, AA 7075-T6 alloy was used as substrate. In this condition, this alloy is very heterogeneous and constituted by Al matrix, second phase particles (hardening precipitates, dispersoids and constituent particles) and grain boundary (GB) regions ($Mg(ZnCuAl)_2$ particles in one side of GB and precipitate free zone (PFZ) or solute depleted zone (SDZ) with depletion of Zn and Cu) [51]. In chloride solutions, this alloy presents two breakdown potentials: the first, at more active potential, is attributed to the dissolution of a very thin mechanically deformed surface layer and the second, at less negative potentials,

attributed to the formation of pits inside the matrix. The dissolution of a very thin layer which is apparently consequence of the mechanical polishing process was demonstrated by an *in situ* observation system [51,52].

The characterization of the microstructure and mechanical behavior showed that the WC-Co coatings obtained by CGS are promising to substitute HVOF coatings; however, the corrosion performance of these coatings must be investigated. Therefore, this work focused on the investigation of the microstructure and corrosion resistance of WC-Co coatings produced by CGS with different feedstock powders WC-12Co and WC-25Co deposited onto AA 7075-T6.

2. Experimental

2.1 Feedstock materials, Substrate, and Reactants

The powder used was a WC-Co cermet with 12 wt% and 25 wt% cobalt content obtained by agglomeration and sintering, processed by Fujimi Inc. (Kiyosu, Japan). Flat (50 mm × 20 mm × 5 mm) and cylindrical (∅ = 25.4 mm and h = 25.4 mm) AA 7075-T6 alloy (0.18wt%Cr, 1.2 wt%Cu, 2.1 wt%Mg, 5.1 wt%Zn and balance Al substrates were degreased with acetone and the surface abraded with P240 SiC paper, which gave a surface roughness, R_a = ~1 µm, were used as substrate. 3.5 wt% NaCl (Sigma Aldrich, 99.8%) aqueous solution prepared with Milli-Q water (18.2 MΩ cm) was used as electrolyte.

2.2 Coating preparation

WC-Co coatings have had the spraying parameters optimized, and were prepared in the Thermal Spray Centre, Barcelona. A Cold Spray Kinetics 4000/17 kW (Cold Gas Technology, Ampfing, Germany) equipment at a maximum operating pressure of 40 bar, temperature of 800 °C, and having nitrogen as the carrier gas was used. A WC based nozzle

(D24) was used to deposit coatings. Initially CGS parameters were optimized to improve the deposition efficiency and adhesion. Pressure was tested from 20 to 40 bar, temperature from 400 to 800 ºC and spray distance values ranging from 10 to 40 mm. Other parameters such as, gun transverse speed, feed rate and spray angle were kept constant. Previous experiments performed, using low temperatures, pressures below 30 bar and distances greater than 30 mm showed deposits with high porosity, poor cohesion between substrate and coating, as well as delamination and the presence of cracks, besides low efficiency to coating deposition. The following coatings were prepared: WC-12Co was prepared using traversing velocity of 100 mm s^{-1}, ratio P/T of 0.037 and one-layer deposition; WC-25Co coatings were sprayed with traversing velocity of 250 mm s^{-1}, ratio P/T of 0.044 and four-layers deposition [9,11].

2.3. Structural, morphological, and chemical characterization

Powders and coatings were characterized by scanning electron microscopy (SEM) using a JEOL JSM-5310 scanning electron microscope coupled to an X-ray microanalysis (EDS) system. The phase composition was analyzed by X-ray diffraction (XRD) using an X-ray diffractometer, SIEMENS model D5000. The particle size distribution of powders was analyzed by Laser Diffraction (LS). The coating thickness was determined in the cross section from SEM images using the Image J software. The porosity of coatings was estimated by analyzing the OM images using the Image J software according to the ASTM E2109-01 (Standard Test Methods for Determining Area Percentage Porosity in Thermal Sprayed Coatings) standard practice.

2.4 Mechanical characterization and hardness test

A sliding wear test was carried out using a ball-on-disk (BoD) method to evaluate the friction coefficient, following the ASTM G99-04 standard. A WC–6Co counterpart ball, a

sample relative velocity of 131 rpm, with a total testing of 1000 m and a force load of 15 N for a radius of 14 mm, were the parameters selected for test purposes. Humidity and temperature were kept below 20% and 25 °C, respectively. The wear tracks produced on the coatings were studied using SEM and Leica confocal equipment for measuring the volume loss of material and to recreate the images of the wear tracks.

Vickers hardness tests were also performed on the cross section of the WC-25Co coating and substrate, according to the ASTM E384-99 standard. The mean values were obtained from at least 15 indentations performed with a load 100 gf for the substrate and of 300 gf both applied for 15 s on the polished cross section of the samples. The hardness test was not performed for WC-12Co coating due to its low thickness, which introduces a great error because the conditions established by the ASTM E384-99 standard practice are not present.

2.5 Corrosion studies

Electrochemical measurements were done using a Gamry Reference 600 systems, in aerated and unstirred 3.5% NaCl solution at (25 ± 1) ºC with a three-electrodes conventional Tait type cell [53]. The reference electrode was Ag|AgCl|$KCl_{3mol/l}$ coupled to a Luggin capillary, Pt-network was the auxiliary and the working electrode was the substrate or coated substrate, fixed at the bottom of the electrochemical cell. The specimen area exposed to the electrolyte solution was 1 cm^2. The corrosion resistance of samples was evaluated by open circuit potential (E_{OCP}) measurements, linear polarization (R_p), potentiodynamic polarization, electrochemical impedance spectroscopy (EIS) and salt spray tests.

The corrosion resistance of samples at short immersion times was evaluated by open circuit potential during 18 h and then R_p were performed applying ±10 mV/E_{OCP} and recorded at 0.166 mV/s. Potentiodynamic polarization curves were also performed after 18 h of E_{OCP} measurements for two samples in the anodic branch with a potential range from - 0.050

V/E_{OCP} to + 0.300 V/E_{OCP}. For the WC-25Co the cathodic branch in the presence and absence of oxygen in solution was also performed, in a potential range from 0.020 V/E_{OCP} to -1.0 V/E_{OCP} at 0.166 mV s^{-1}. The Stern-Geary equation was used to obtain the corresponding R_p values from i_{corr} and the Tafel slopes b_a and b_c.

EIS and E_{OCP} were also monitored for relatively long immersion times: (a) AA 7075-T6 substrate 196 h; WC-12Co 600 h and WC-25Co 700 h of immersion. EIS measurements for coated samples were performed at 1 h and every 24 h of immersion, in the frequency range from 100 kHz to 5 mHz, by applying a sinusoidal potential perturbation of 10 mV rms on E_{OCP} with 10 points/frequency decade. All experimental data were tested for consistency with the Kramers-Kronig transform (KKT) available in the GAMRY system software. The Equivalent Electrical Circuit (EEC) using the Z-view® software was employed for quantitative analysis of the EIS responses.

Salt spray tests of as-deposited WC-Co coatings were performed in a neutral 5 wt% NaCl at 35 °C for 1000 h, in accordance with ASTM B117-11 Standard Practice. As no signals of corrosion of WC-25Co were observed up to 1000 h, time established by the Standard Practice, the salt spray test was continued to a total of 3000 h.

3. Results and discussion

3.1 *Structural, morphological, and chemical characterization*

The LS analysis showed that the particles sizes of both powders have a size range from +8-26 µm and a mean particle size of (15±2) µm (Fig 1S (a) and 1S (b), supplementary data, *SD*). SEM images of the free surface (Fig. 1a and 1c) shows that both powders had similar spherical morphology and were fairly uniform obtained from an agglomeration and sintering process. SEM images of the cross section powders shows particles randomly distributed into the matrix (Fig. 1b and 1d). EDS analysis (Fig. 2S, *SD*) shows that the

particles are WC because the area is rich in tungsten and the other dark phase around the WC grains is cobalt. Cobalt works as a binder.

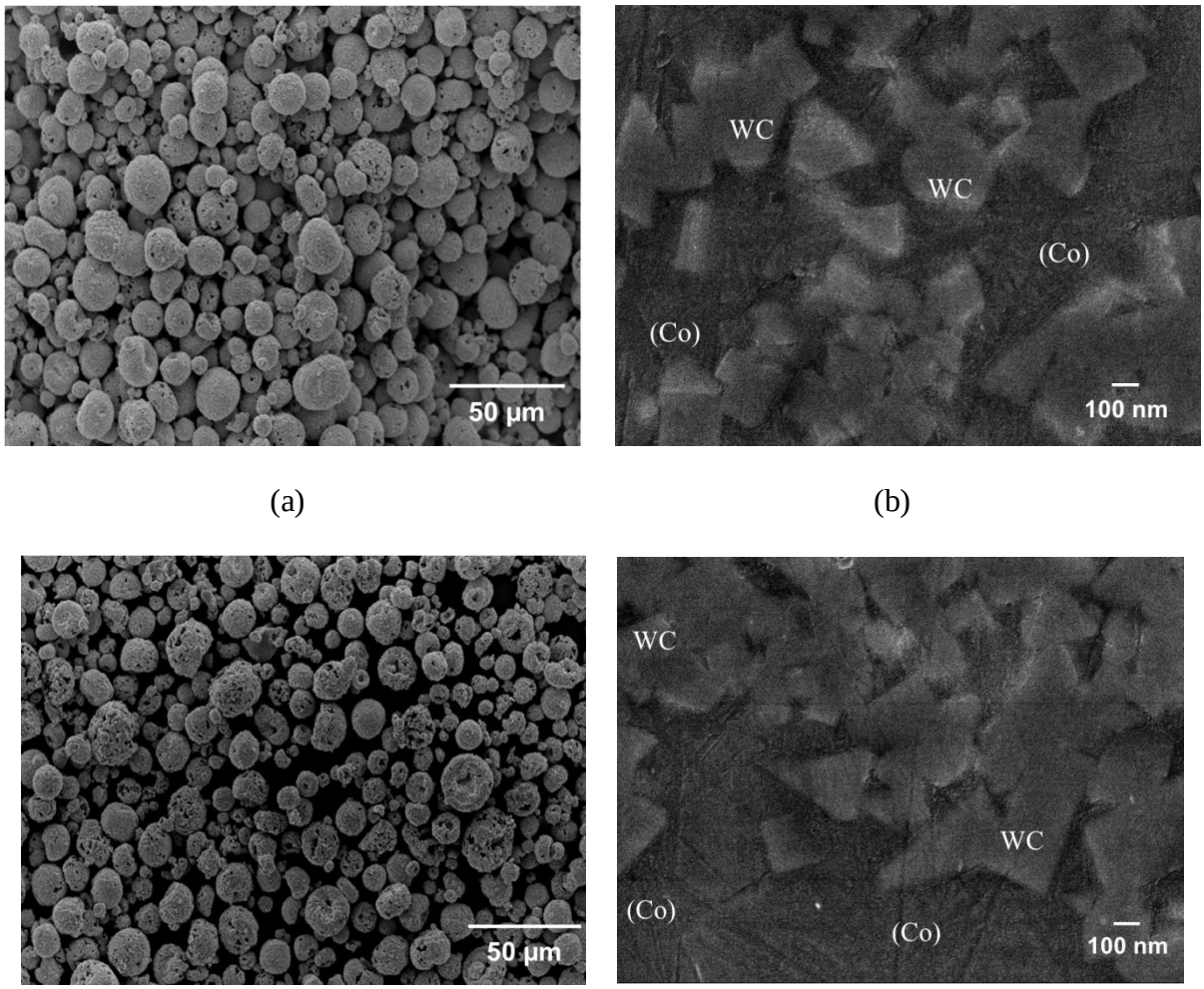

Fig. 1. SEM images of the feedstock powders: (a) free surface of WC-12Co powder, (b) cross section of WC-12Co powder, (c) free surface of WC-25Co powder and (d) cross section of WC-25Co powder.

XRD patterns (Fig. 2) for the feedstock powder and coatings showed the same characteristic peaks. WC and Co phases were observed while W_2C, W, Co_6W_6C and Co_3W_3C phases, normally formed when the material undergoes high oxidation or partial degradation, were absent. Therefore, there were no changes in the material composition, and the obtained

coatings were homogeneous and almost oxide-free, as well as the starting materials. As CGS uses high kinetic energy and low thermal energy during the spraying process, the coatings formed are almost free of oxides and chemical reactions which may lead to the formation of new phases do not occur [48,49,54].

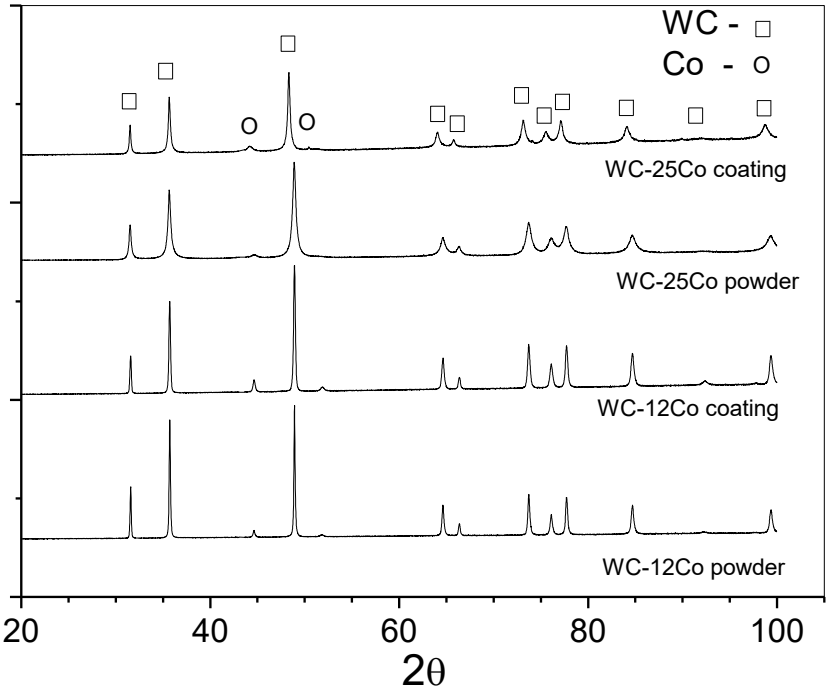

Fig. 2. X-ray diffractograms for powders and coatings.

Fig. 3 shows SEM images of cross section and polished surface of WC-Co coatings. The SEM analysis of the cross section shows a typical microstructure of cold sprayed coatings, where the particles are severely deformed, and metallic oxides, cracks and interconnected porosity are not observed at the metal/coating interface and along all the coating [55]. The top layer of coatings was less compact than the bottom layer, which agrees with the literature [56] that describes the CGS coatings as mainly consisting of a top layer with some porosity and a dense bottom layer. The porosity of coatings was estimated to be (0.7±0.1)% for WC-12Co and (0.4±0.1)% for WC-25Co samples, which may reflect a different behavior in electrolyte solution. The as-prepared substrate surface had a roughness

around 0.5 μm and after spraying the roughness of the coating/substrate interface increased to ≈12 μm because the WC-Co particles are harder than the substrate and, therefore, they can deform the substrate during spraying. This would improve the coating/substrate bonding. The SEM images of polished surfaces (Fig. 3b and 3d) show two distinguishable WC and Co phases. EDS analysis confirmed that the bright phase is WC phase and the dark one is cobalt.

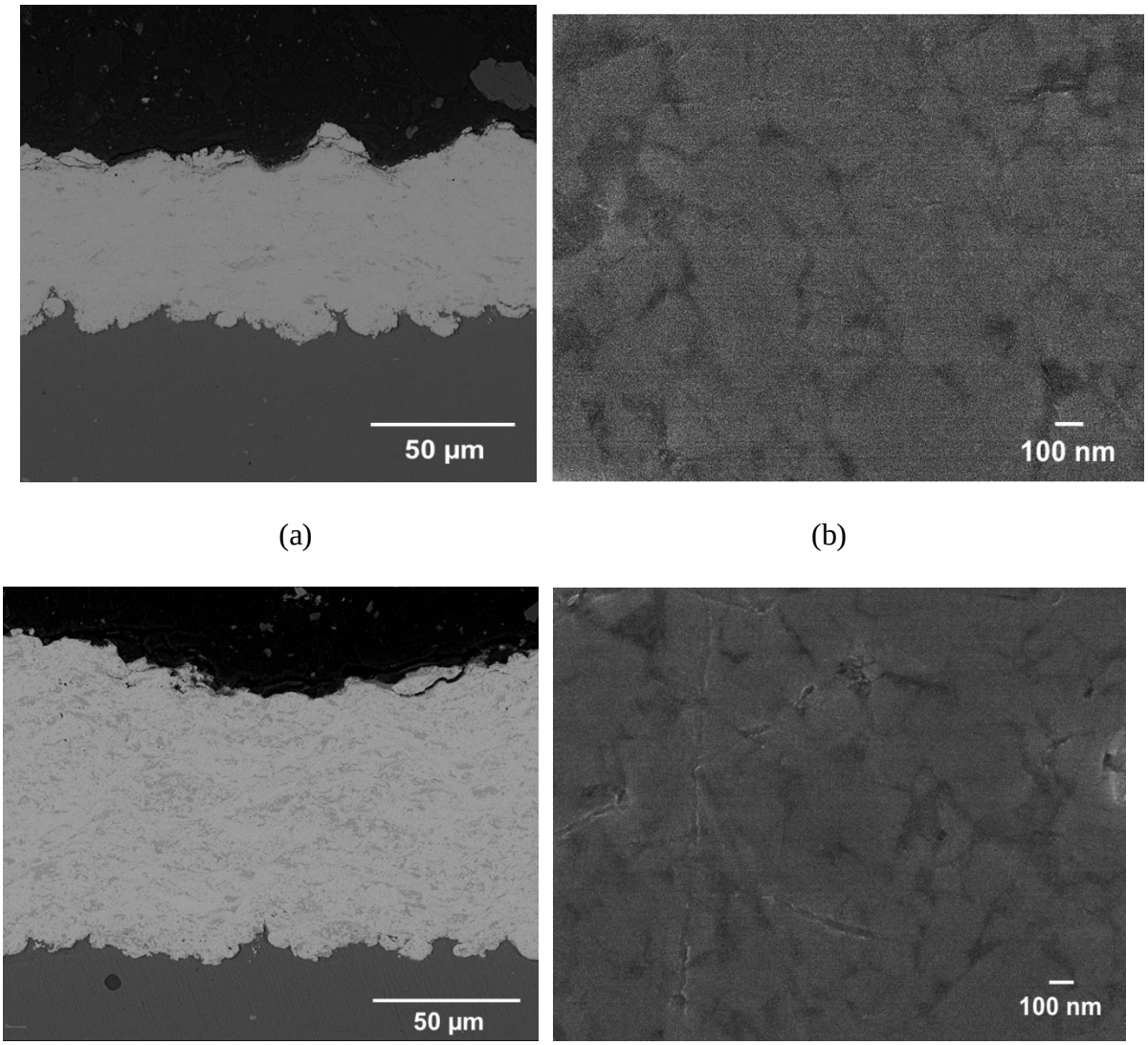

Fig. 3. SEM imagens of WC-Co coatings onto AA 7075-T6. (a) WC-12Co cross section, (b) WC-12Co polished surface, (c) WC-25Co cross section and (d) WC-25Co polished surface.

The distribution of WC particles in the Co binder was uniform, which can improve the wear resistance of the WC-Co coatings [11]. The thickness was (65±5) μm for WC-12Co and (118±6) μm for WC-25Co. WC-12Co coating showed lower thickness because one layer of material was sprayed and when more than one layer was applied, the deposition became a challenger because it was difficult for the WC-12Co powder to deform onto the previously deposited WC-Co. The rebound particles, cavitation of the pre-deposited layer and crack formation were some problems observed when more than one layer was tried to be deposited. Other studies have also reported difficulty in the deposition of multilayer WC-Co coatings [9,45,57,58]. Kim et al. [45] deposited two layers of WC-12Co coating by spraying and using different spray parameters, but all coatings showed interconnected porosity and cracks. WC-12Co powder is known to be difficult to deposit by cold spray due to the low ductility of the WC phase [59]. Therefore, it is difficult to reach the critical particle velocity for WC–Co in addition to the intrinsic high critical velocity for cold spray deposition. Studies have shown that when the ceramic content increases in the feedstock powder the overall deposition efficiency decreased because of the in-flight particle interactions and the deflection of particles from the substrate [10,11,59].

On the other hand, WC-25Co particles have lower hardness and are more ductile due to the lower content of WC phase and the higher proportion of cobalt binder. Therefore, several layers of powders can be sprayed without problems of deflection of the particles.

3.2. *Mechanical characterization and hardness test*

The friction wear resistance of the CGS coatings was tested two times with different samples under a load of 15 N and initial roughness surface values of 8 μm. Wear track profilometric measurements were performed using a confocal laser technique to quantify the material lost, measure the path diameter and to get the shape of wear profile (Fig. 4).

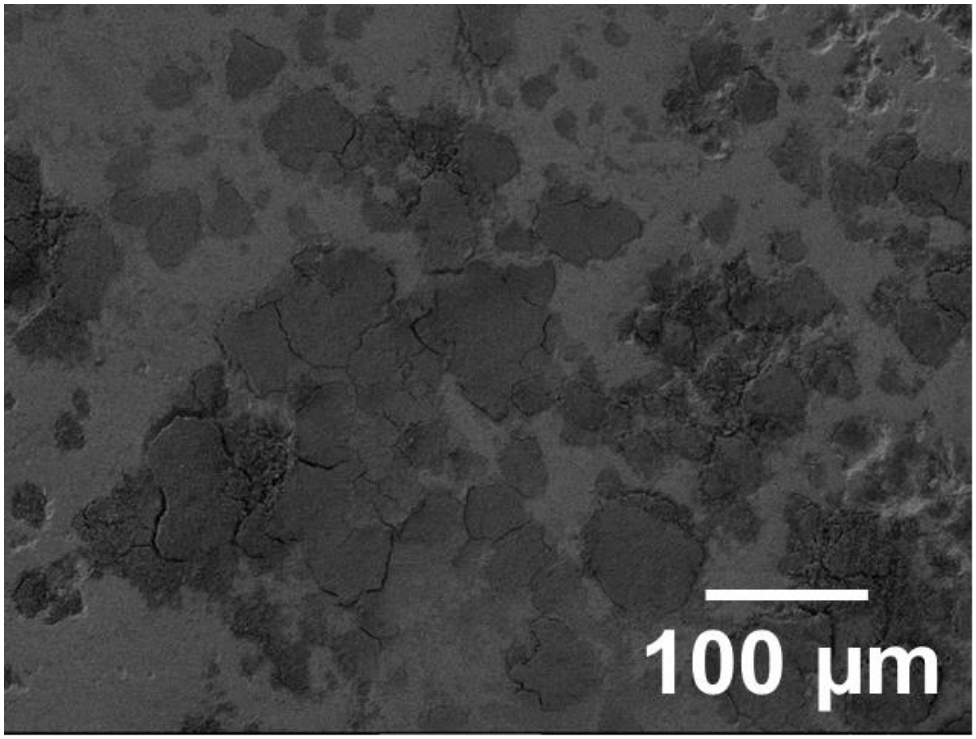
100 µm

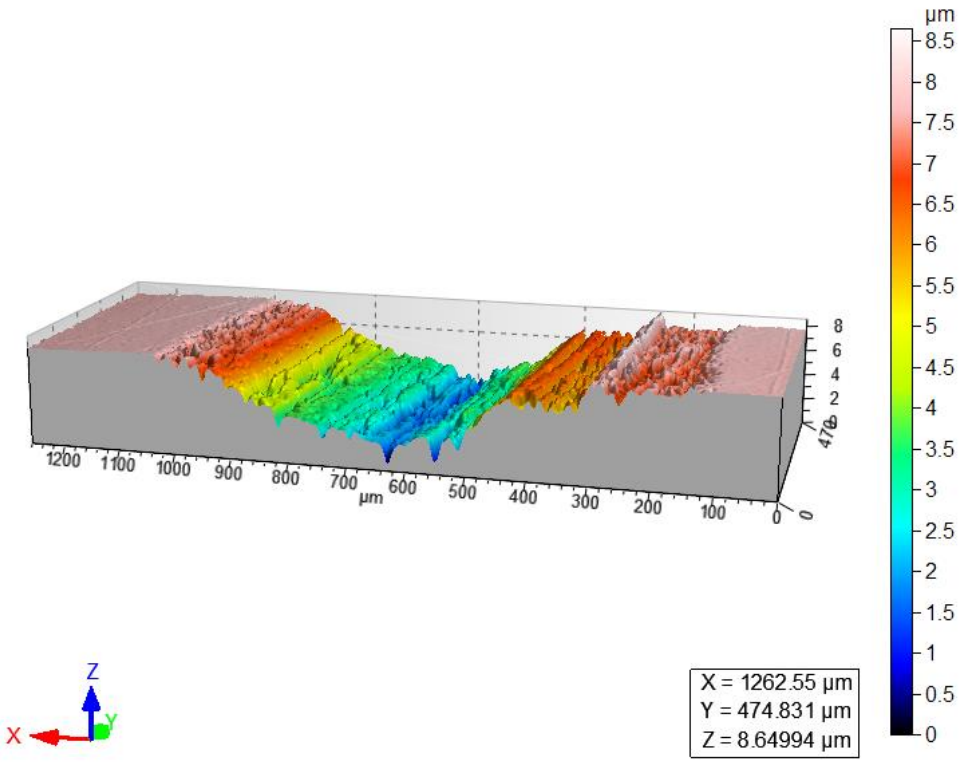
µm
8.5
8
7.5
7
6.5
6
5.5
5
4.5
4
3.5
3
2.5
2
1.5
1
0.5
0
1200
1100
1000
900
800
700
600
500
400
300
200
100
0
µm
8
6
4
2
0
Z
X
Y
X = 1262.55 µm
Y = 474.831 µm
Z = 8.64994 µm

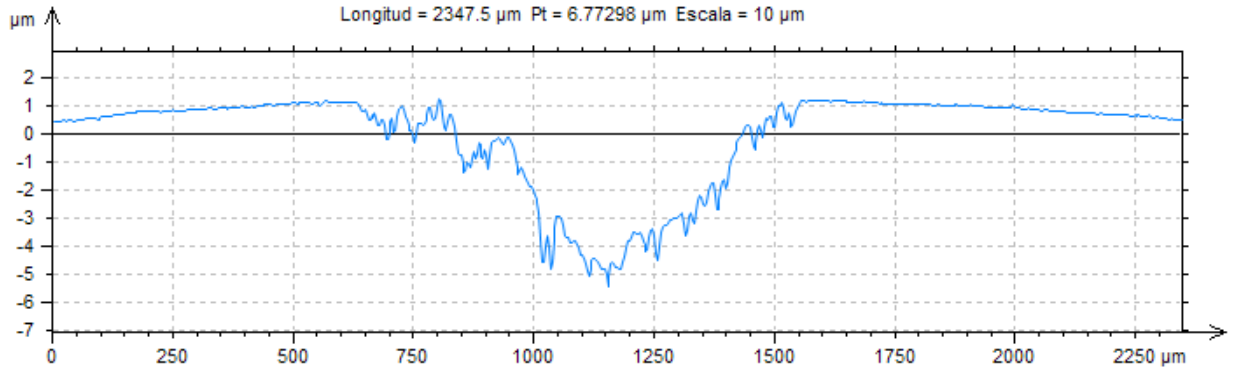
Longitud = 2347.5 µm Pt = 6.77298 µm Escala = 10 µm
µm
2
1
0
-1
-2
-3
-4
-5
-6
-7
0
250
500
750
1000
1250
1500
1750
2000
2250 µm

(a)

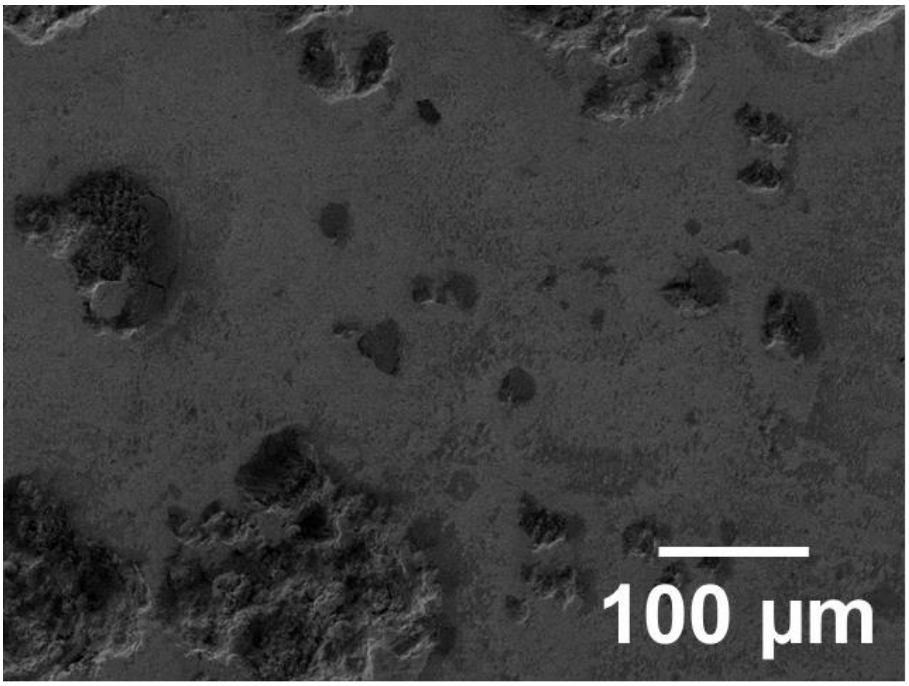
100 µm

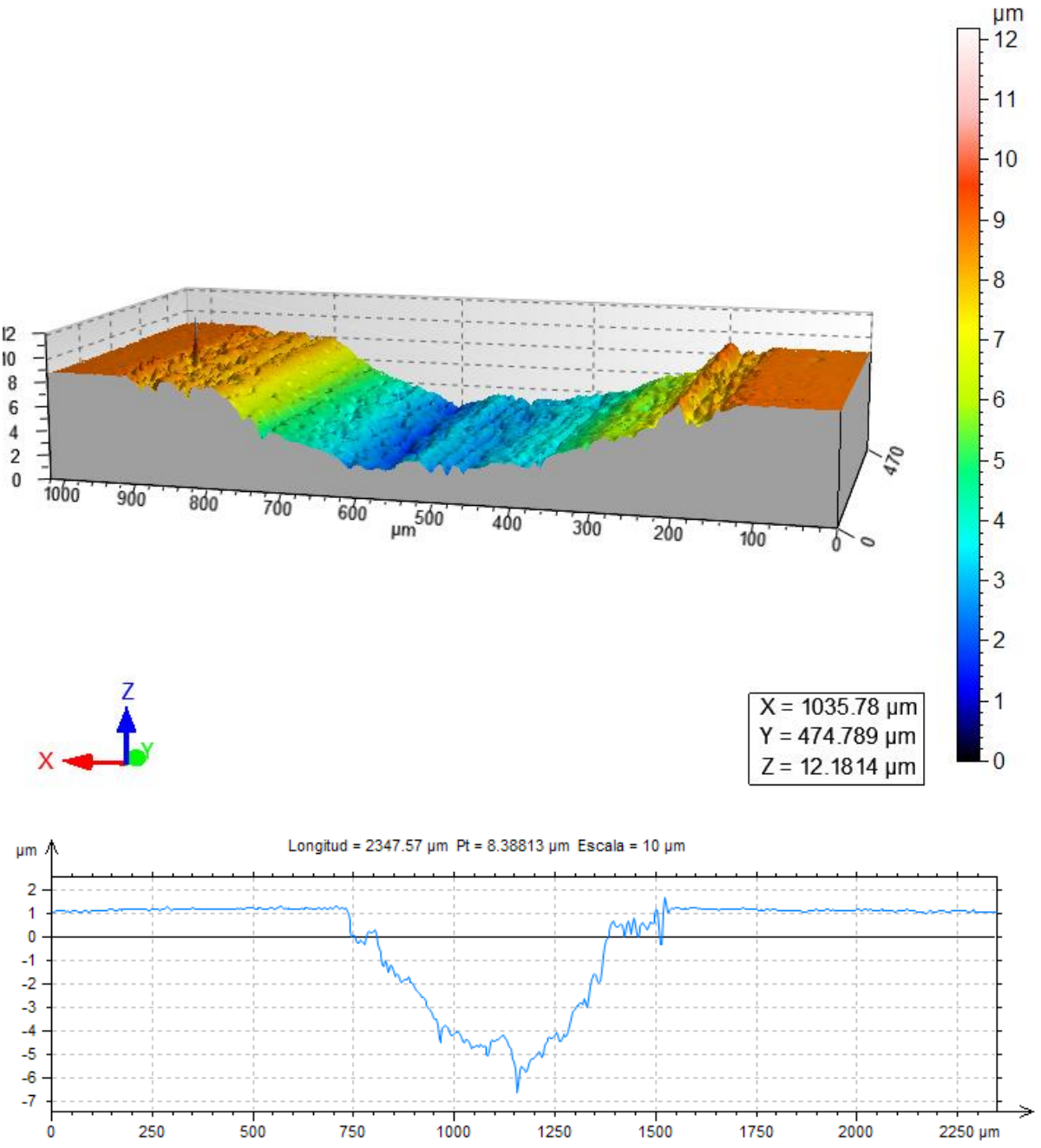

(b)

Fig. 4. Morphological features of the wear tracks of the cold spray: (a) WC-12Co and (b) WC-25Co.

After a sliding distance of 1000 m onto the WC-12Co surface coating, the volume lost was 1.3×10^{-5} mm^3/N - 1.1×10^{-5} mm^3/N and the wear track was ≈810 µm – 808 µm (Table 1). SEM images (Fig. 4a) after the sliding test showed small loss of material and debris formation

at the wear track, which indicates the presence of W and Co lubricant oxides because of the high temperatures achieved during sliding. EDS analysis of debris at specific points along the wear path confirmed the presence of WC and Co oxides that are responsible for the lubricant effect, and can explain the wear resistance and almost no material loss [9].

Table 1. Main wear properties of WC-Co coatings.

Parameter	WC-12Co	WC-12Co	WC-25Co	WC-25Co
[1]Friction coefficient	0.50	0.47	0.45	0.46
[1]Volume loss / mm^3/Nm)	1.3×10^{-5}	1.1×10^{-5}	1.7×10^{-5}	1.9×10^{-5}
[1]Wear track depth / µm	810	808	830	837

[1]The deviation was obtained determining the average of two measures and calculating the standard deviation.

The WC-25Co coating showed a different wear mechanism. SEM images of the wear tracks of coatings showed that particles are pulled out from the coating surface and small areas with lubricant oxides (Fig. 4b). The wear mechanism seems to begin with the extraction of carbides from the matrix, even though the binder phase acts as an excellent support for carbides and oxides formation due to the abrasion [9]. For WC-25Co coating, the volume lost was 1.7×10^{-5} mm^3/N - 1.9×10^{-5} mm^3/N and the wear track was 830 µm - 837 µm (Table 1). Due to the WC carbide particle distribution in the ductile binder and absence of brittle or fragile phases, a very high sliding resistance was achieved for all coatings. The wear resistance during testing proved to be higher to sample with low Co amount (WC-12Co) due to the greater amount of the ceramic phase, in agreement with Couto *et al.* [11].

The hardness of the substrate AA 7075-T6 was 162±3 HV_{100} similar to the value given in [60,61]. The hardness of WC-25Co coating 754±1 HV was like that obtained for the same coating prepared by CGS technology and higher than HVOF coating [9,12]. The WC-12Co

coating probably has higher hardness than WC-25Co one due to the higher content of the WC phase as it was reported in another study [62], however, the thickness of our WC-12Co coating was not enough to allow measuring the hardness properly.

3.3 Electrochemical corrosion studies

3.3.1 Open circuit and polarization studies

First it will be discussed electrochemical results obtained at short immersion times. Fig. 5 shows the E_{OCP} curves in NaCl 3.5% for 18 h of immersion. For the AA 7075-T6 alloy substrate, E_{OCP} values were between -0.7 to -0.8 V/Ag|AgCl|$KCl_{3mol/l}$ typical values for aluminum alloys in chloride solution containing oxygen [63,64], and tends to stabilize around -0.78 V/Ag|AgCl|$KCl_{3mol/l}$. Small potential oscillations were observed that can be related to the attack of oxide layer by chloride ions and repassivation of the surface [65].

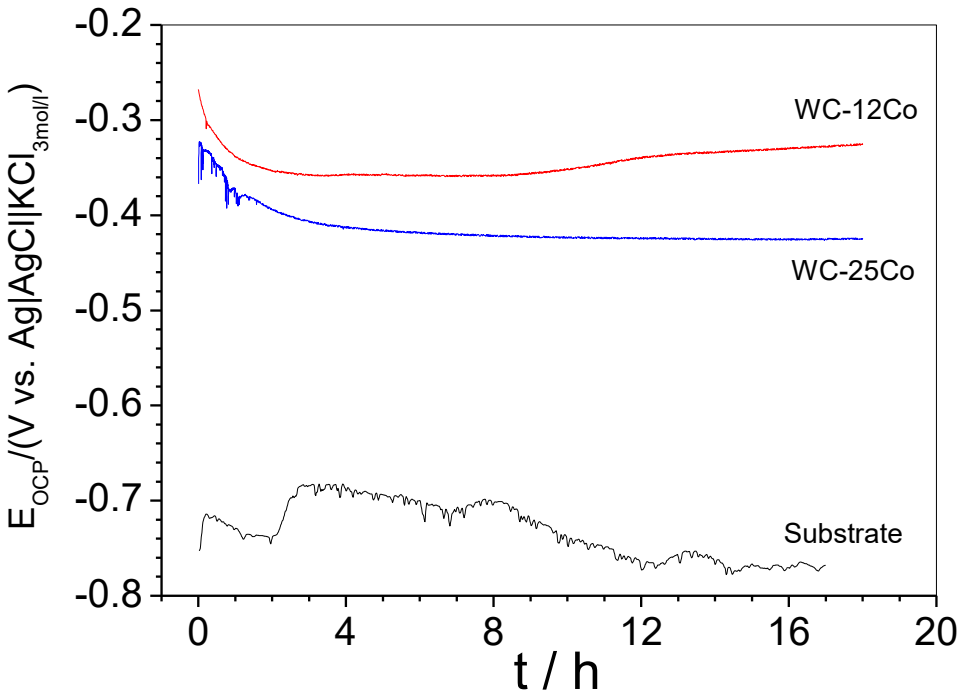

Fig. 5. Open circuit potential *vs.* time for all studied samples measured in aerated and unstirred 3.5 wt% NaCl solution for relatively short immersion times, at 25 ºC.

For as-sprayed WC-Co coatings, the E_{OCP} behavior was completely different from the AA 7075-T6 substrate. Initially, E_{OCP} values decreased due to the oxides dissolution from the sample surface, chloride adsorption, change in the local concentration of oxygen or metal ions on the surface [10], and then stabilize around -0.32 V/Ag|AgCl|$KCl_{3mol/l}$ (WC-12Co) and -0.42 V/Ag|AgCl|$KCl_{3mol/l}$ (WC-25Co). At E_{OCP} conditions the behavior of the WC-Co cermets is dominated by dissolution of the less noble component, pure metallic cobalt, and by the selective dissolution of the metal from the binder phase (Co + WC) [7,14, 66,67]. The exposed metallic phase oxidizes since at the beginning of the immersion while the reduction of dissolved O_2 occurs mainly at the WC phase. Galvanic coupling with the WC component of the material may enhance the dissolution rate of the Co binder from the coating, and the hydrolysis of the metal cations can acidify the solution inside regions where access of oxygen is limited creating conditions to accelerate the cobalt corrosion [14,66]. On the other hand, the reduction of oxygen on the carbide phase increases the local pH and due to the relatively high distance between anodic and cathodic sites, the increase of the pH on the cathodic regions may destabilize the carbide surface [14].

R_P values were estimated from linear polarization measurements after 18 h in 3.5% NaCl solution and given in Table 3. Higher R_P and $E_{i\rightarrow 0}$ values were obtained for the sample with lower cobalt content. Table 3 also shows E_{corr} and i_{corr} values obtained from the potentiodynamic polarization curves by extrapolation the Tafel lines.

A slightly increasing of current density for the sample with higher binder content was also previously observed [68]. Therefore, the WC-12Co sample seems to show the best performance among the studied coatings to protect the aluminum alloy substrate against corrosion in chloride solution at short times, since it presented the most positive E_{corr} and the lowest corrosion current density value. It is true that the higher E_{corr} value points in that direction, but the lowest current density for WC-12Co sample can also be related to the small

relative area of the binder (around 18% estimated from images analysis) when compared to WC-25Co sample with an estimated relative area of the binder around 32%.

Table 3. Corrosion parameters estimated from linear and potentiodynamic polarization curves.

Parameter	AA 7075-T6	WC-12Co	WC-25Co
$^{*}R_p$/kΩ cm^2	7.2±2	2.3±0.1	1.5±0.1
$^{*}E_{i\rightarrow 0}$/mV/$_{Ag\|AgCl\|KCl3mol/l}$	-814±2	-326±4	-425±2
E_{corr}/mV/$_{Ag\|AgCl\|KCl3mol/l}$	-831±2	-336±2	-425±1
i_{corr}/μA cm^{-2}	1.4±0.2	1.4±0.2	3.2±0.3
$^{b}i_{corr}$/μA cm^{-2}	0.60	1.1	2.8
$^{c}i_{corr}$/μA cm^{-2}	1.4	1.4	3.1
b_a /mV dec^{-1}	82.5	31.9	28.5
b_c/mV dec^{-1}	40.4	36.1	51.9
$^{a}R_p$/kΩ cm^2	25±4	9.5±0.2	3.9±0.1

*From small amplitude linear polarization, *R*p value was the average of two samples with 3 curves each sample.

[a]Cathodic polarizations were performed and the R_p and i_{corr} values were obtained as explained in Supplementary data.

[b] i_{corr} values obtained from Tafel plots.

[c] i_{corr} values obtained from Stern-Geary equation.

Fig. 6 shows the anodic polarization curves for all coatings and substrate. AA 7075-T6 shows E_{corr} = -0.75 V/Ag|AgCl|KCl$_{3mol/l}$ and i_{corr} ~1.5 μA cm^{-2}. For the substrate, the polarization curves show a rapid increasing of current when the potential reaches the values of -0.70 V/Ag|AgCl|KCl$_{3mol/l}$ due to pitting corrosion. The first breakdown potential described in [51,67] is poorly observed even considering that the substrate surface was mechanically treated, however the pitting potential is well-defined at -0.72 V/Ag|AgCl|KCl$_{3mol/l}$. Anodic and cathodic processes of aluminum corrosion in chloride medium at pH near 7 are,

respectively, dissolution of aluminum and reduction of dissolved oxygen, according to the following reactions (1-4) [65]:

$$Al \rightarrow Al^{3+} + 3e^{-} \quad (1)$$

$$O_2 + 2H_2O + 4e^{-} \rightarrow 4OH^{-} \quad (2)$$

Hence, Al^{3+} ions may react with OH^{-} ions to form aluminum hydroxide near the aluminum surface according to the global equation (3).

$$Al^{3+} + 3OH^{-} \rightarrow Al(OH)_3 \quad (3)$$

The aluminum hydroxide can precipitate on the surface due to its low solubility product and may change gradually to aluminum oxide, resulting in the formation of a passive film:

$$2Al(OH)_3 \rightarrow Al_2O_3 + 3H_2O \quad (4)$$

This normally occurs on aluminum or aluminum alloys surfaces, but it cannot necessarily happen on aluminum composite surface. For composites, in generally, this kind of oxide film does not cover the entire electrode surface and/or offer sufficient protection against attack of chloride anions, inducing aluminum dissolution when it is exposed to the corrosion solution. This explains the rapid increase of current when high overpotentials are achieved.

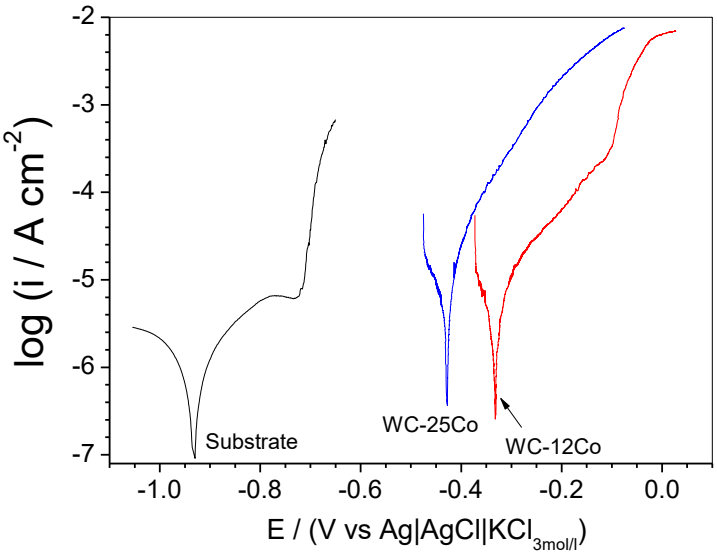
log (i / A cm-2)
-2
-3
-4
-5
-6
-7
-1.0
-0.8
-0.6
-0.4
-0.2
0.0
E / (V vs Ag|AgCl|KCl3mol/l)
Substrate
WC-25Co
WC-12Co

(a)

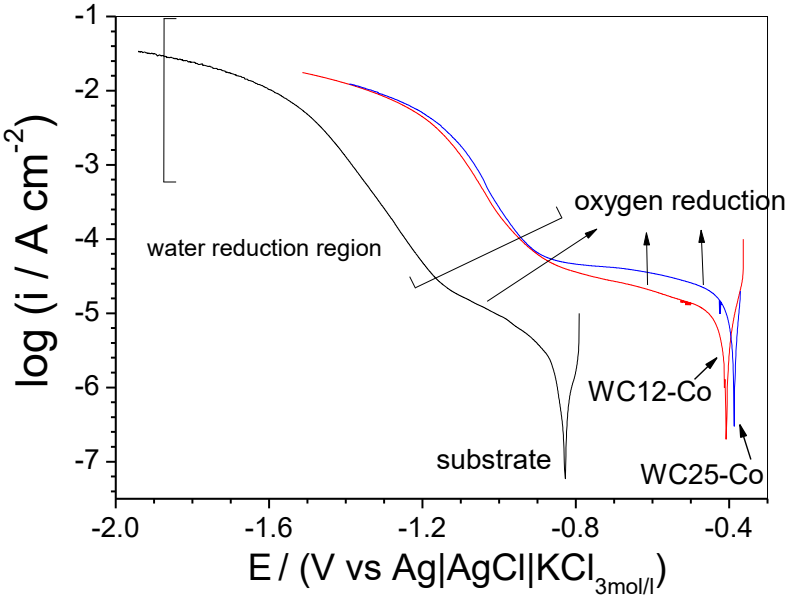
log (i / A cm-2)
-1
-2
-3
-4
-5
-6
-7
-2.0
-1.6
-1.2
-0.8
-0.4
E / (V vs Ag|AgCl|KCl3mol/l)
water reduction region
oxygen reduction
WC12-Co
substrate
WC25-Co

(b)

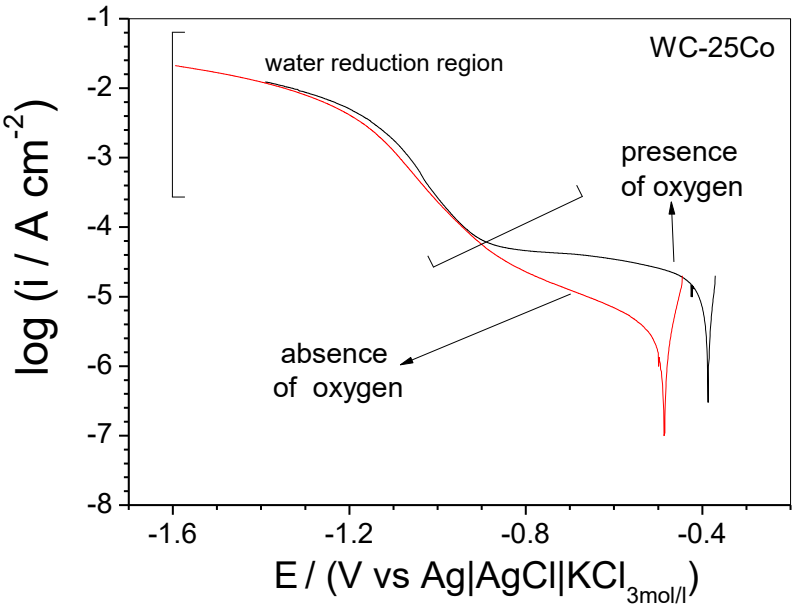

(c)

Fig. 6. (a) Anodic and (b) cathodic potentiodynamic polarization curves of AA 7075-T6 alloy and coated samples recorded in non-deaerated and quiescent 3.5 wt% NaCl solution at 0.166 mV/s and after ~18 h of immersion. (c) Cathodic curves of WC-25Co coating obtained in the same solution in the presence and absence of oxygen.

The anodic polarization measurements for coatings (Fig. 6a) show a gradual current increase as a more positive overpotential is applied. The corrosion potential of WC-12Co coating shifted to more positive values, E_{corr} =-0.33 V/Ag|AgCl|$KCl_{3mol/l}$, and i_{corr} =1.2 µA cm^{-2}, while the corrosion potential of WC-25Co coating was -0.42 V/Ag|AgCl|$KCl_{3mol/l}$ and i_{corr} 2.9 µA cm^{-2}. These values are slightly lower than those E_{corr} values obtained for WC-Co with similar composition in 0.5 mol/l H_2SO_4 [68] and 0.05 mol/l NaCl aqueous solutions [66]. Anodic and cathodic processes of WC-Co corrosion in chloride solution correspond to the following reactions: dissolution of Co (eqn. 5) and reduction of dissolved oxygen (on WC phase, eq. 2) [14,66].

$$Co \rightarrow Co^{2+}_{(aq)} + 2e^- \quad (5)$$

In the absence of oxygen and aggressive anions, during the anodic polarization various metallic oxides may be formed on the WC-Co surface. Co is being oxidized to CoO, forming an inner layer, and to $Co_{3-x}O_4$ as an outer layer [14,34,70]:

$$Co + 3H_2O \rightarrow CoO + 2H_3O^+ + 2e^- \quad (6)$$

$$Co + 4H_2O \rightarrow Co(OH)_2 + 2H_3O^+ + 2e^- \quad (7)$$

$$3CoO + 3H_2O \rightarrow Co_3O_4 + 2H_3O^+ + 2e^- \quad (8)$$

$$3Co(OH)_2 \rightarrow Co_3O_4 + 2H_3O^+ + 2e^- \quad (9)$$

$$Co_3O_4 + 6H_2O \rightarrow 3Co(OH)_3 + H_3O^+ + e^- \quad (10)$$

However, in the presence of chloride ions the formation of such oxides is not able to make the surface passive due to the high chloride activity. At open-circuit conditions or at small positive applied potentials, the binder phase undergoes selective dissolution, but when higher potential is applied the dissolution of the WC phase also takes place [14]. Cathodic curves (Fig. 6b) obtained in the presence of oxygen showed two plateaus of current which were attributed to the reduction of oxygen, in the range from -0.5 to -0.9 V/Ag|AgCl|$KCl_{3mol/l}$, and to the reduction of water at more negative potentials. Fig. 6c compares cathodic curves in the absence and presence of oxygen. In the presence of oxygen, a fast-electrochemical reaction (diffusion control) is observed, while in its absence, the reduction of water with hydrogen evolution was the main process observed (equation 11).

$$2H_2O_{(l)} + 2e^- \rightarrow H_{2(g)} + 2OH^-_{(aq)} \quad (11)$$

Both cathodic reduction of water or oxygen shifts the solution local pH towards higher values. An investigation on the pH-dependent of the WC phase demonstrated its instability in the alkaline pH 9-14 range, which might make it susceptible to chemical dissolution according to equation (12) [14,71]:

$$WC + 6H_2O \rightarrow WO_4^{2-} + CO_2 + 12H^+ + 10e^- \quad (12)$$

At a more negative potential than -1.0 V/Ag|AgCl|$KCl_{3mol/l}$, the hydrogen evolution (reduction reaction of water) and the carbide dissolution occur, leading to an increase of the current.

Cross section SEM images after anodic potentiodynamic polarization (Fig. 3S, *SD*) shows that a brittle zone is formed inside the coatings embracing all the cross section for WC-12Co sample (Fig. 3S (a), *SD*) and 10 to 30 µm from the top of WC-25Co (Fig. 3S (b) *SD*), in which cracks are easily developed during the cross section preparation. The increase in the defects of sample with less cobalt can be related to the lower binder content and the higher porosity. The applied potential has favored the increase of stress in this region due to the acceleration of the growth of oxides and electrolyte penetration, but the bottom of the coating was not affected by the polarization.

The substrate (AA 7075-T6) and coatings were also examined by E_{OCP} measurements for long immersion times: AA 7075-T6 substrate (196 h), WC-12Co (~600 h) and WC-25Co (~700 h). For AA 7075-T6 (Fig. 7) the E_{OCP} value at 1 h of immersion was around -0.85 V/Ag|AgCl|$KCl_{3mol/l}$ and increase to -0.64 V/Ag|AgCl|$KCl_{3mol/l}$. This observation indicates that oxide formation occurs on the substrate surface when exposed to corrosion solution [66 72]. However, this oxide film is not enough protective and at 24 h the potential decreased to

around -0.9 V/Ag|AgCl|$KCl_{3mol/l}$, due to localized corrosion, and for longer immersion times maintained around -0.85 V/Ag|AgCl|$KCl_{3mol/l}$ until 196 h.

For the coatings E_{OCP} values decreased in the first hours of immersion (Fig. 7), which may indicate the dissolution of native oxides present at the surface due to the adsorption and attack of chloride ions. After 48 h of immersion the potential was around -0.44 V/Ag|AgCl|$KCl_{3mol/l}$ (WC-12Co) and -0.42 V/Ag|AgCl|$KCl_{3mol/l}$ (WC-25Co), probably due to the formation/dissolution of corrosion products, mainly dissolution of cobalt. E_{OCP} value suggests that the electrolyte does not reach the substrate in the first hours of immersion, as suggested by the potential of the substrate is around ~-0.85 V/Ag|AgCl|$KCl_{3mol/l}$.

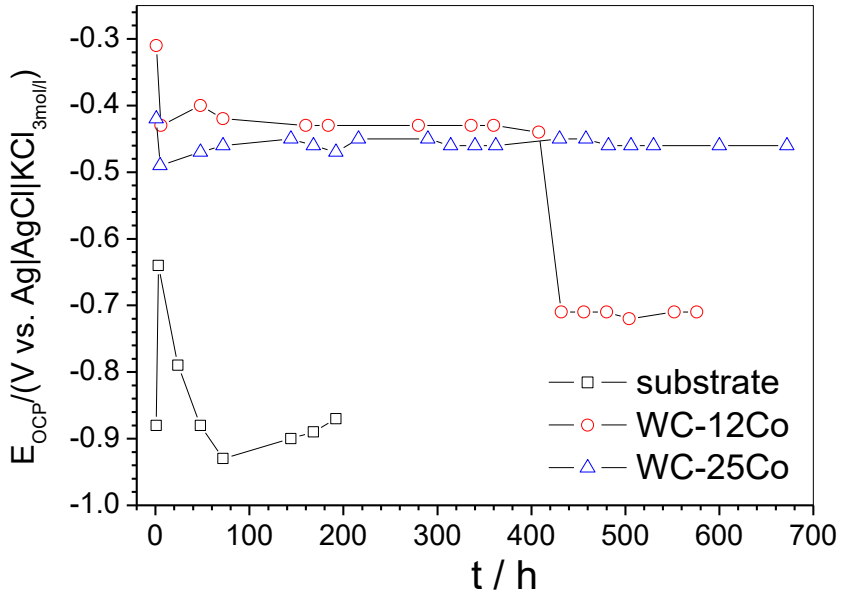

Fig. 7. Open circuit potential *vs.* time for all studied coatings measured in aerated and unstirred 3.5 wt% NaCl solution for long immersion times, at 25 ^{o}C.

For understanding the corrosion process which takes place at open circuit potential during long immersion times, microscopic inspection of the surface of WC-Co coating was performed before the immersion in 3.5% NaCl and after 96 h (Fig. 8). Image analysis shows

an almost oxide-free coating which can explain the initial decrease in the value E_{OCP} at short times. The formation/dissolution of corrosion products mainly on the surface near WC particles where chloride ions adsorb onto the cobalt (binder) can explain the small variation of potential. Small defects of coatings mainly surrounding the WC particles and galvanic effect assist the accelerated dissolution of Co phase at specific sites (Fig. 8b) generating deep attack at these areas (Fig. 8c (B)) as was observed before [66]. A comparison between the cross section SEM images at 20 μm from the top for both coatings and at the end of E_{OCP} measurements (Fig. 4S, *SD)* shows great holes for WC-12Co indicating higher damage of this coating and supporting the hypothesis used below to explain EIS results. Corrosion around the WC phase can be explained, as usual, by the formation of local cells between the WC phase (nobler) and the Co matrix (more active) [68]. No signs of corrosion were observed on WC after 96 h of immersion, but it may take place for longer exposure times since the local pH becomes alkaline due to the oxygen reduction [66,67]. The Co dissolution preferentially occurs and may cause the fall out of WC particles, even if they are insoluble (Fig. 8c (C)). The result is a rough appearance of the surface (Fig. 8a). The dissolution of the Co phase and the loss of WC particles can form interconnected porosity and paths which allow the electrolyte diffusion throughout the coating until the substrate. This fact and the lower thickness of WC-12Co explain the fast decrease of the E_{OCP} value for this sample after 400 h of immersion (Fig. 7), reaching -0.71 V/Ag|AgCl|$KCl_{3mol/l}$, a value very close to that obtained for the substrate, suggesting that the electrolyte may have reached the substrate.

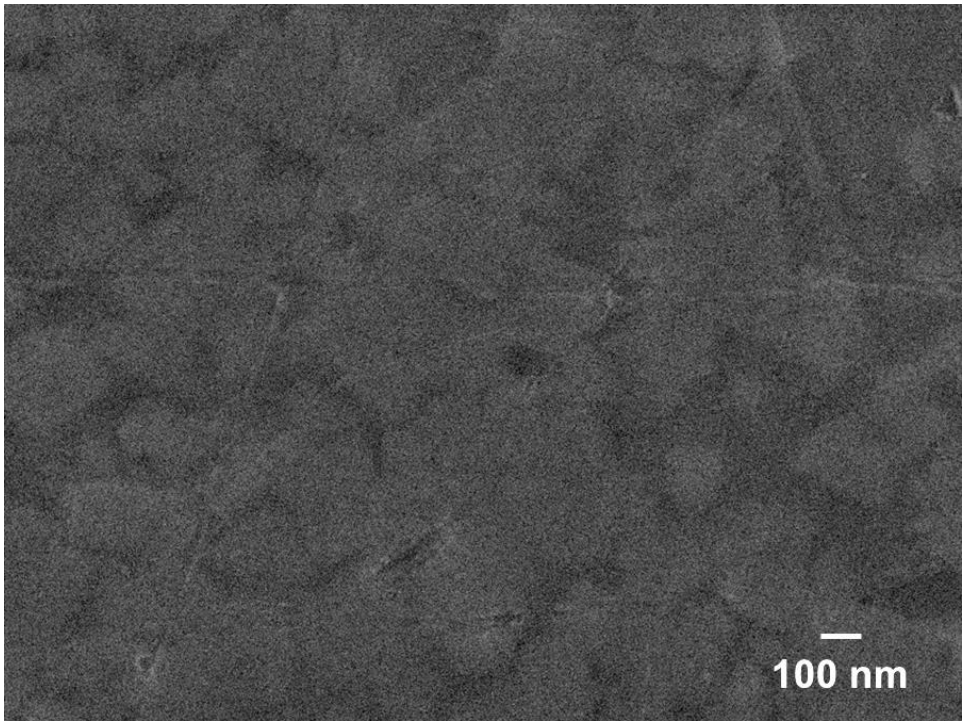

(a)

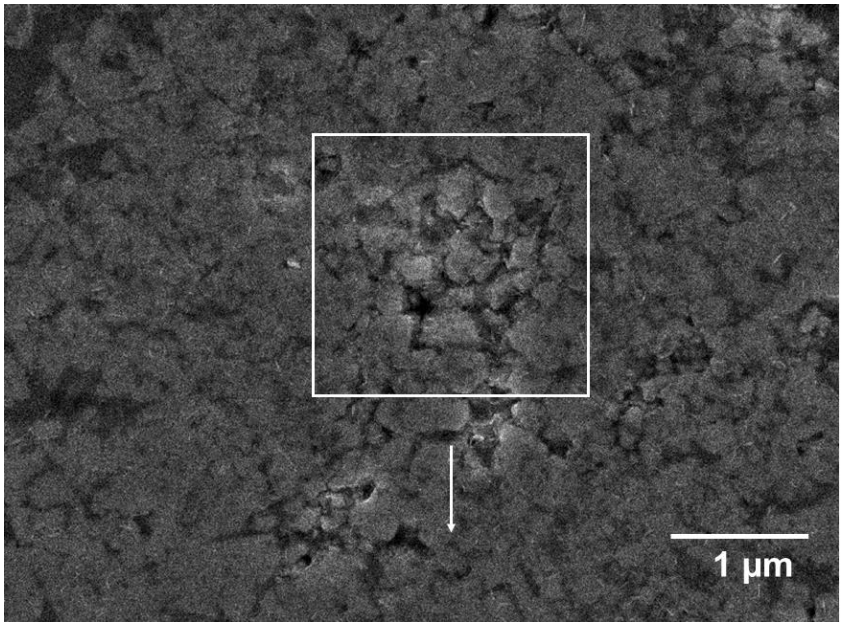

(b)

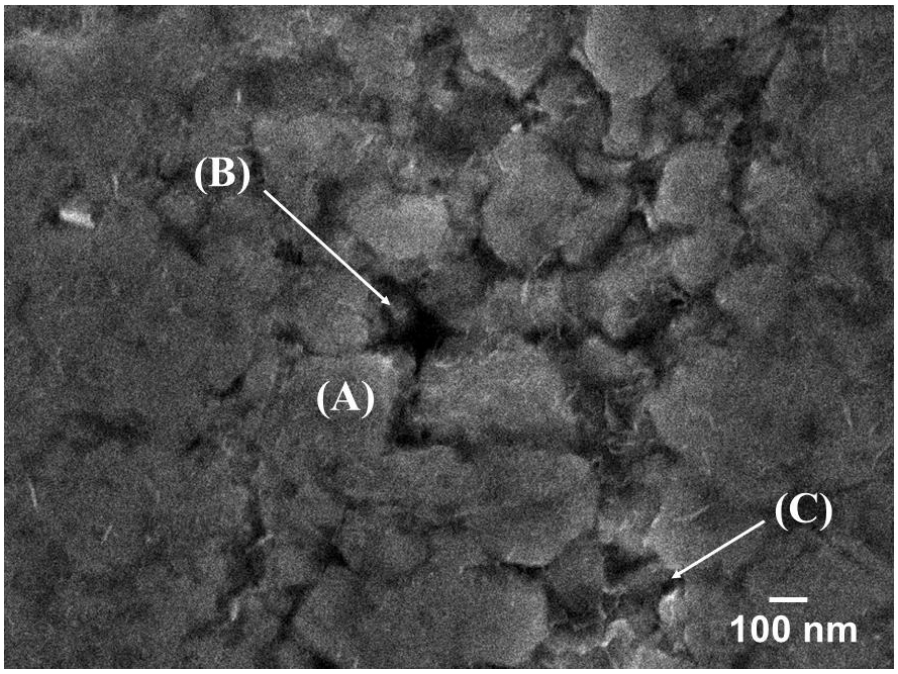

(c)

Fig. 8. (a) SEM images of the WC-12Co coating polished surface, (b) SEM images of the corroded area after 96 h of immersion in 3.5% NaCl and (c) The same region of b with higher magnification: (A) intact WC particles, (B) deep attack to specific sites of cobalt phase and (C) loss of the WC particles.

SEM cross section images of WC-12Co coatings show that the top of the coating underwent a severe damage. The coating was damaged in a great extension with pathways, which allow the electrolyte to reach the substrate in some specific points, but not all over the coating/substrate interface (Fig. 9a). EDS analysis at the spots 1 and 2 detected the following elements at spot 1: oxygen (3 wt%), cobalt (24 wt%), tungsten (70 wt%) and a small amount of aluminum (3 wt%); at spot 2 oxygen (5 wt%), Co (20 wt%) and W (75 wt%). Oxygen content is greater near the surface, and the percentage of cobalt decreases due to higher metal dissolution at the top of the coating. This indicates that a larger area has been attacked at the top than other regions of the coating. It is important to note that the top of the coating presents higher porosity and the roughness is significantly higher than to the substrate. The presence of

aluminum at some spots indicates that the electrolyte has reached the substrate only at some areas and not at all the coating/substrate interface.

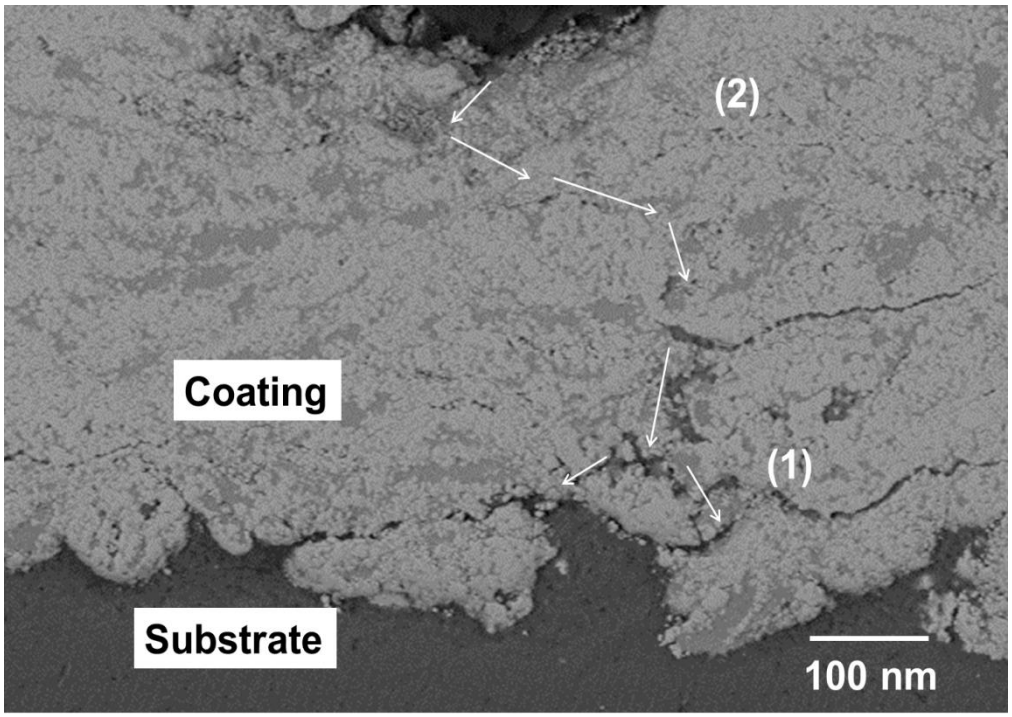

(a)

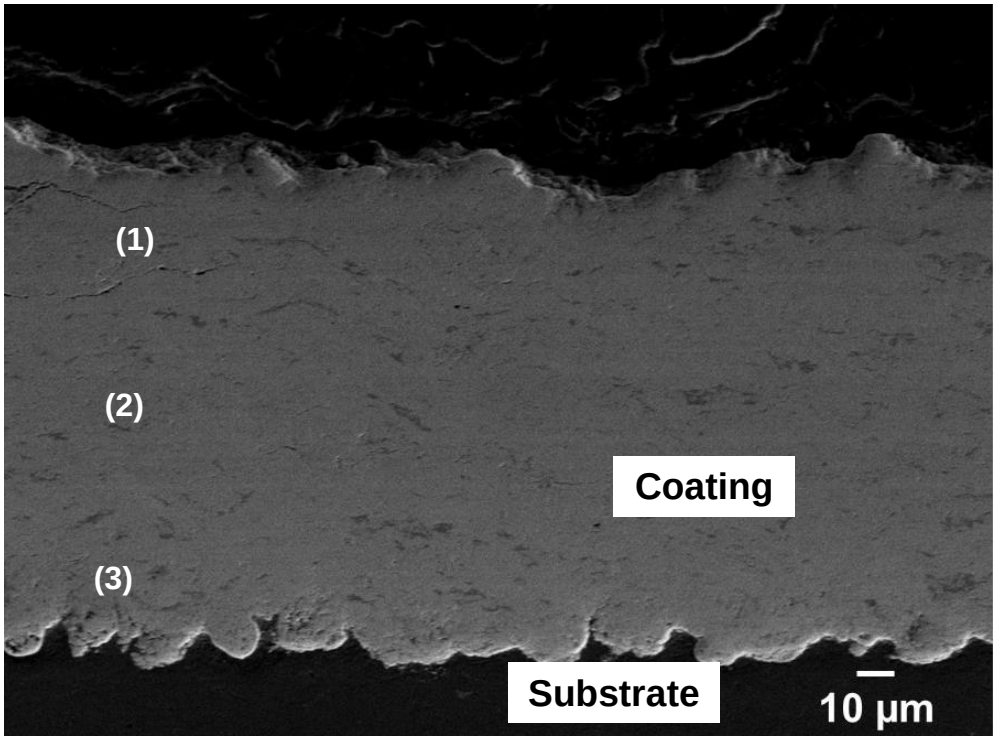

(b)

Fig. 9. Cross section SEM images of (a) WC-12Co coating after 600 h and (b) WC-25Co coating after 700 h in 3.5 wt% NaCl. The numbers in (a,b) show the spots areas where EDS analyses were performed.

For WC-25Co coating the E_{OCP} values remained constant even after 700 h of immersion. After the test, the SEM cross section images for WC-25Co (Fig. 9b) showed no corrosion of the substrate probably due to the higher coating thickness than WC-12 Co. It can be seen only small amount of oxides near the top surface. Some cracks are observed inside the coatings, 40 µm from the top, probably developed during the cross section preparation. EDS analysis (Fig. 5S, *SD*) of the corroded cross section (Fig. 9b) revealed only tungsten, carbon, cobalt and oxygen. Aluminum was not detected, indicating that the electrolyte did not reach the substrate even after ~700 h of immersion.

3.3.2. Electrochemical impedance studies

Electrochemical impedance spectroscopy measurements were performed for all samples with 24 h interval for different immersion times depending on the response of the coating. WC-12%Co coating was studied up to 600 h because the open circuit potential suggested degradation of the coating at around 400 h. Figs. 10-12 show EIS diagrams that illustrate the impedance behavior of the samples in chloride solution for different times: 1 h, 96 h and 192 h for AA 7075-T6 (Fig. 10), and at 24 h and at 500 h of immersion for both coatings (Figs. 11 and 12). Solid lines correspond to the fitting of the impedance data.

For the substrate at 1 h the complex plane apparently shows only one time constant that suggests being related to the native aluminum oxide response, while at $t \geq 24$ h of immersion two time constants seems to appear (Fig. 10a) which could be related to the charge transfer process due to the aluminum oxidation and oxygen reduction, and to the response of

corrosion products. For some impedance diagrams and at low frequency (LF) dispersion with indication of inductive behavior is observed due to the instability of the system caused by the pitting development (Fig. 6S, *SD*). The Bode - ϕ *versus* log (f) plots shows a large maximum centered at 25 Hz with a phase angle around -80º, which is typical of a capacitive system, and small difference in the Bode modulus of impedance *versus* frequency is observed in LF region with the immersion time (Fig.10b).

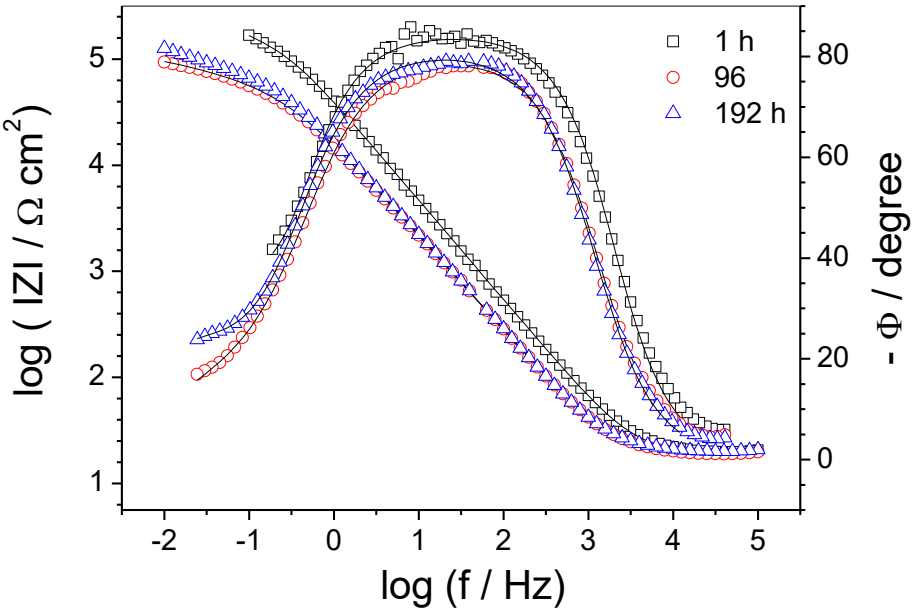

Figure 10. (a) Experimental (symbol) and fitting (solid line) Bode phase plots obtained for the substrate during different immersion times in 3.5 % NaCl solution at 25 ºC.

For the coatings, the complex plane plots at 24 h show one asymmetric and incomplete semicircle, but for the WC-12Co coating a second time constant seems being appearing at low frequency (Fig. 11a). The Bode - ϕ *versus* log (f) plots show one larger time constant in the range of medium frequencies (MF) to low frequency range (LF) (Fig. 11b). The shape of this plot suggests the presence of more than one time constant, which was verified when treating

the experimental data using equivalent electrical circuits. For the two coatings, Bode - ϕ *versus* log (*f*) graphics (Fig. 11b) depict the maximum of the phase angle at -57º (~0.3 Hz). At short immersion times seems that no great difference exists between the impedance values of the two samples as can be observed from the modulus of impedance.

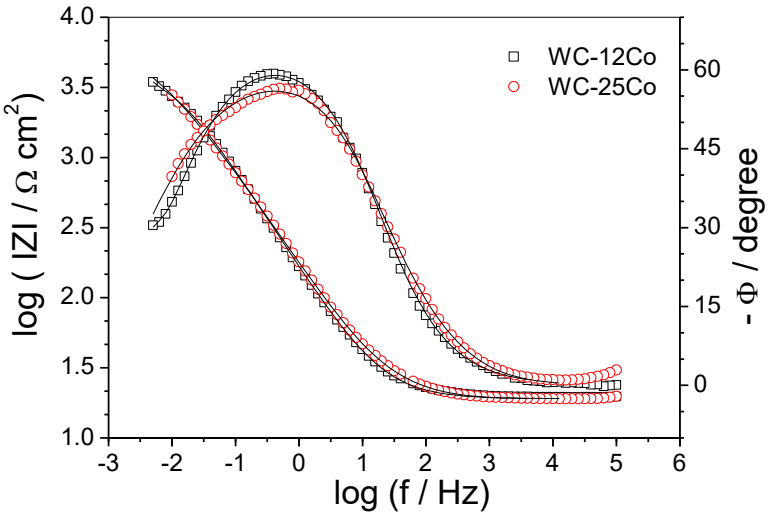

Fig. 11 - (a) Experimental (symbol) and fitting (solid line) Bode phase plots obtained for the coated samples for 24 h of immersion in 3.5 wt% NaCl solution at 25 ºC.

Fig. 12 shows EIS diagrams illustrating the impedance behavior of the coatings in chloride solution for ≈500 h of immersion. The complex plane plots show two asymmetric semicircles for the samples with greater amplitude for WC-25Co coating. The Bode - ϕ *versus* log (f) plot show two time constants: the first at MF and the second not very well defined at LF. Bode ϕ *versus* log (f) diagrams for WC-12Co shows a phase angle of -44º while for WC-25Co the phase angle value is -57º, like that obtained during the initial immersion period. The decrease of the capacitive arc and phase angle values suggests that the WC-12Co coating has its resistance decreased, which was attributed to the electrolyte accessing to the substrate through the defects of the coating. On the other hand, the WC-25Co coating shows no

decrease in the resistance. This can be attributed to the higher barrier effect of the coating due to its greater thickness. As mentioned earlier, the WC-25Co particles are more ductile, and during the spraying process a greater plastic deformation of the particles occurs upon the impact with the substrate or already deposited layers. This provides an increase in the deposition efficiency and the formation of a more compact and thick coating, resulting in better corrosion performance [9].

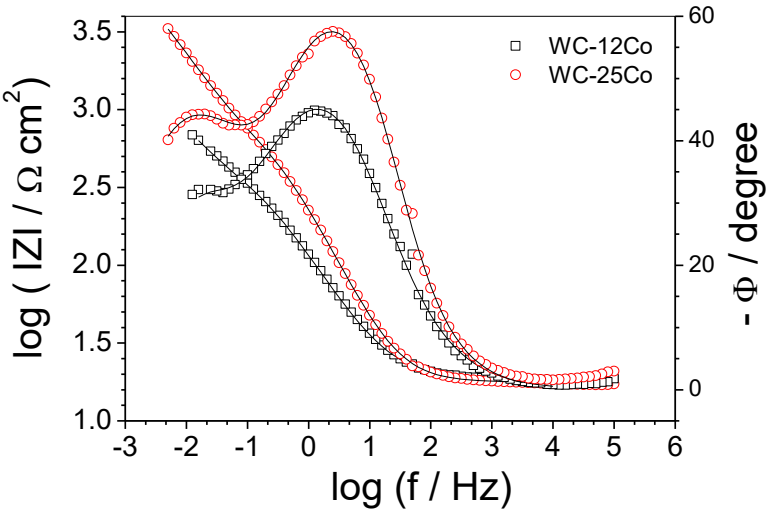

Fig. 12 - (a) Experimental (symbol) and fitting (solid line) Bode phase plots obtained for coated samples after ≈600 h of immersion in 3.5 wt% NaCl solution at 25 ºC.

The EIS results were also quantitatively analyzed using the equivalent electrical circuit (EEC) theory and EECs were chosen considering the structure of the samples, the best fitting of experimental data and the lower residual error of each parameter from the equivalent circuit.

For the AA 7075-T6 alloy an EEC with the solution resistance in series with two in parallel time constants (Fig. 13a) was used to fit EIS data for some immersion times and the fitting parameters are in Table S1 (supplementary material). In this circuit, R_s is the solution resistance and CPE_{ox}//R_{ox} represents the constant phase element (CPE_{ox}) of the aluminum

oxide in parallel with the resistance (R_{ox}) that comprises the resistance of the oxide film and the resistance of the solution inside the pores of the film. The constant phase element (CPE) represents a non-ideal capacitor, that means a resistance when the exponent n=0, an ideal capacitor (n=1), a Warburg (n=0.5) and an ideal inductor (n=-1) [73]. CPE_{dl}//R_{ct} represents, respectively, the capacitance related to the charge of the electric double layer and the charge transfer resistance due to the anodic and cathodic processes: oxidation of Al from the matrix and reduction of oxygen on the intermetallic compounds. The CPE_{dl}, like before, substitute the ideal capacitor for an interface with heterogeneous charge distribution on the surface and n is the exponent. At 1 h the resistance of the film is great due to the presence of a highly resistant native aluminum oxide film, and for longer immersion times the film is damaged by the aggressive attack of chloride ions, causing a decrease in the resistance. As the native film is degraded, a new film is formed by the corrosion products and the resistance increases again, but is lower than the observed for the native oxide film (Table S1, supplementary material). The n values are near 0.9 which are expected for a heterogeneous film. R_{ct} values follow the same tendency of R_{ox}, but the n_{ct} values decreased from 0.9 to around 0.5 suggesting some diffusion through the film of corrosion products, probably of chloride ions.

For the coatings, the following observations were considered to choose and justify the equivalent electrical circuit: (a) the oxide content detected on the electrode surface is very low, even at the end of the experiment as demonstrated by the EDS analysis (Fig. 5S). It means that under the conditions here studied the main processes are dissolution of cobalt (from the binder) and reduction of oxygen (on WC particles); (b) sign of passivation was not observed for both coatings and for all immersion times and then, cobalt is continuously dissolved. Some metallic regions dissolve faster originating sites like pits (Fig. 8b) that can continuously undermine the coating and the attack can also propagate laterally [66]; (c) oxygen is mainly reduced at the electrode surface because the access to the inner regions of

the sample is limited [66**]**. As consequence, the local pH can increase at long immersion times and destabilizes the cathodic surface (WC phase); (d) the electrolyte apparently did not reach the substrate until around 400 h for WC-12wt%Co coating and ~700 h for WC-25wt%Co coating, as indicated by the high open circuit potential values for both coatings at that immersion times (Fig. 7); (e) after 500 h of immersion, for WC-12wt%Co coating, EDS analysis detected Al and some alloying elements at specific points near the substrate, meaning that the solution crossed all the substrate at specific regions (Fig. 9a), which is also suggested by the sharply decreased of E_{OCP} after 400 h (Fig. 7). The WC-25Co coating/substrate interface remained intact (Fig. 9b) and Al and alloying elements were not detected inside the coating near the substrate, which indicate that the solution did not reach the substrate during the immersion time. By the same reason, the E_{OCP} remained constant for all the immersion time (Fig. 7).

The dissolution of metallic cobalt can be accelerated because the hydrolysis of the Co^{2+} ions acidifies the medium locally [74], increasing the deep dissolution of cobalt in some places of the binder and corrosion underneath the surface, may extend it laterally to the surface. The reduction of oxygen at the cathodic sites (WC phase) may increase the local pH considering that they are separated from the anodic ones, which could facilitate the WC dissolution [14,66].

The observations described above on the characteristics of the studied system and the literature [14,66-68] allowed interpreting our EIS data in a similar way that was recently applied for cemented carbides [66] by adopting the EEC of Figure 13b and 13c. In these circuits, a constant phase element (CPE) substitutes the capacitor to account for the effect of the heterogeneities of charge distribution at the electrode surface [73].

At short immersion times, the systems respond with one time constant and considering that, practically, oxides are absent, the only process occurring would be the oxidation of the

cobalt from the binder and the reduction of oxygen on the WC phase, which are represented by two in parallel R_{ct}//CPE_{dl} sub-circuits which stand for the cathodic and anodic charge transfer resistance and electric double layer of cathode and anode. Then, they are reduced to one *R*//*CPE* sub-circuit (Fig. 13b). However, this simple circuit can embrace all contributions arising from the global surface such as resistances and capacitances associated with the charge transfer process and contributions from an incipient film existing or one eventually formed by the accumulation of corrosion products on the surface. This simple sub-circuit may be represented as R_{surf}//CPE_{surf} that is dominated by the lowest resistance and the greatest capacitance of processes developing at the surface. After some time, 24 h for instance, a new time constant is required to fit the experimental results, which was also observed for WC-Co composite and cemented carbides by Oliveira *et al*. [66]. This second time constant was attributed to the rapid dissolution of cobalt from the binder at specific sites, i.e., at some defect of the binder or points surrounding the WC phase where the galvanic effect can accelerate the cobalt dissolution, producing holes (Fig. 8b). The holes become increasingly deep and the attack to the binder may propagate laterally through defects between splats increasing the damage to the coating. Thus, the solution inside holes adds a new resistance (R_{dh}) to the system separating the process occurring inside the holes from that at the surface. Therefore, the R_{ct}//CPE_{dl} sub-circuit accounts for the dissolution of cobalt inside the holes and within the coating, and the system may be described by circuit in Fig. 13c. As the experiment progresses R_{dh} increases in relation to R_{surf} and when $R_{surf} < R_{dh}$ the EEC in Fig. 13c changes to that in Fig.13d. In our study, it seems that $R_{surf} < R_{dh}$ after around 24 h of immersion, therefore, our EIS data obtained after 24 h of immersion were fitted with EEC shown in Fig. 13d and the parameters values of the different elements of the circuits employed for the coatings are given in Tables S2 and S3 (supplementary material). In this circuit R_s represents the solution resistance. The suitability of the proposed EECs was indicated by the Chi-squared

deviations (χ^2) values, which are around 10^{-4}, the relative low standard errors (<10%) of each parameter (Table S2 and S3, Supplementary material), as well as the good agreement between the fitted and experimental EIS diagrams (Figs. 11,12). An EEC like that shown in Fig. 13d was also previously used to treat impedance data obtained for CGS zinc coating applied on mild steel substrate [75].

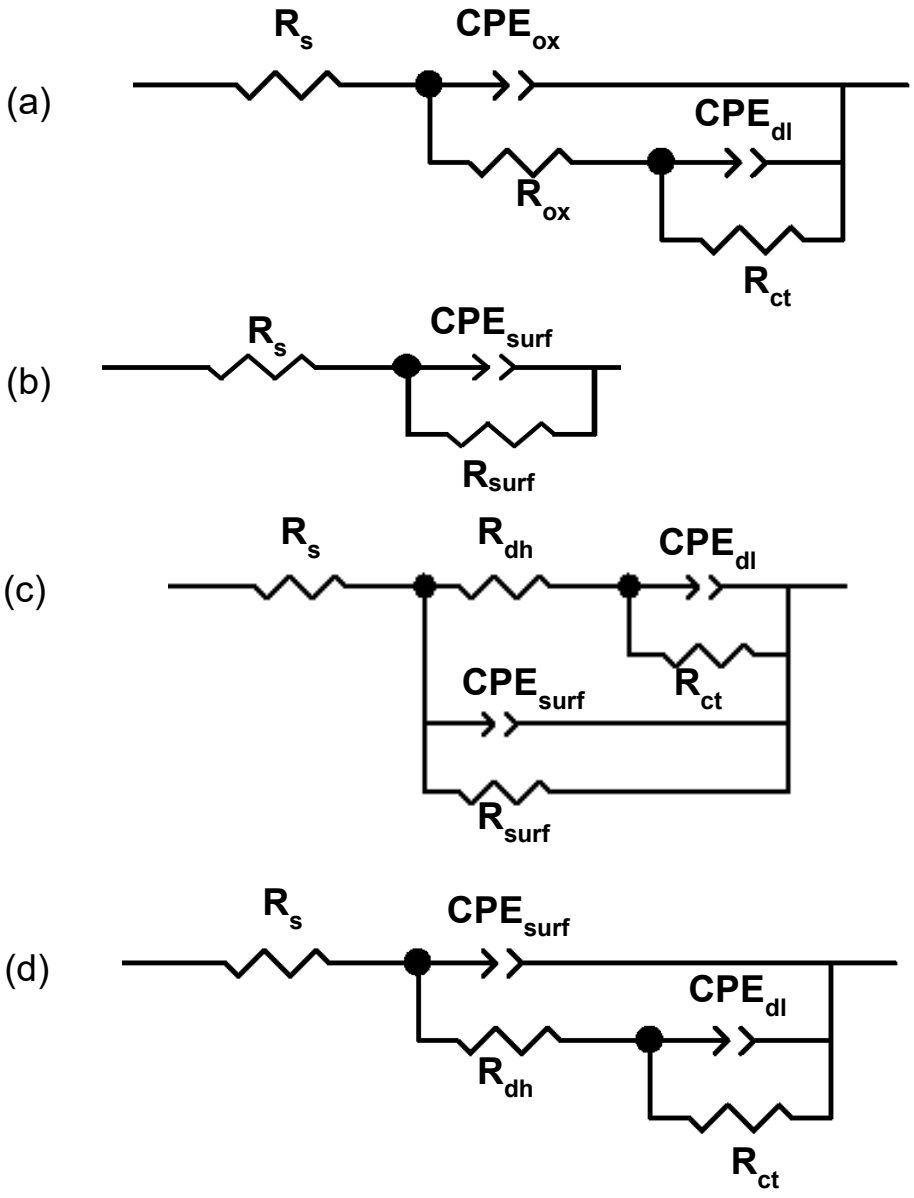

Figure 13. Equivalent electrical circuits (EECs) used to analyze the impedance data: (a) substrate; coatings (b) for the first hours of immersion; (c) interpretation of EIS data after some immersion time and (d) EEC used to fit EIS data after a few hours of immersion.

Given that only the cobalt is dissolved, the polarization and charge transfer resistance can be recalculated to consider only the dissolution area: ~18% and ~32% for WC-12Co and WC-25Co, respectively. This recalculation can give R_p and R_{ct} values closer to the expected to the cobalt dissolution areas during the first hours of immersion; this procedure has been used before [14,64,67] with the same purposes. However, it should be taken with caution for longer immersion times because the area where cobalt is dissolved becomes difficult to be estimated due to the development of holes and attack to other defects of the coating. On the other hand, since that R_{surf} was removed from the EEC (Fig.13d) and the correction has not been considered anymore, the contribution of the surface to the total cobalt dissolution resulted of minor significance. Figure 14 depicts the R_{ct} and R_{dl} corrected values for both coatings, and a great decrease in both resistances is noticed at around 400 h of immersion for WC-12Co while for WC-25Co the resistance continuously tends to increase.

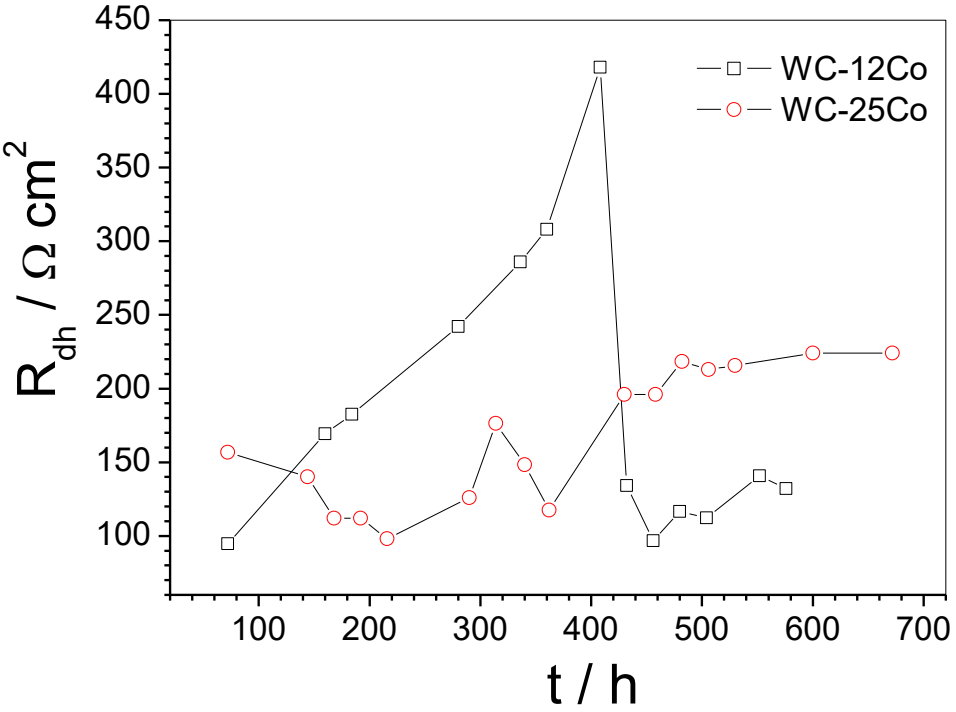

(a)

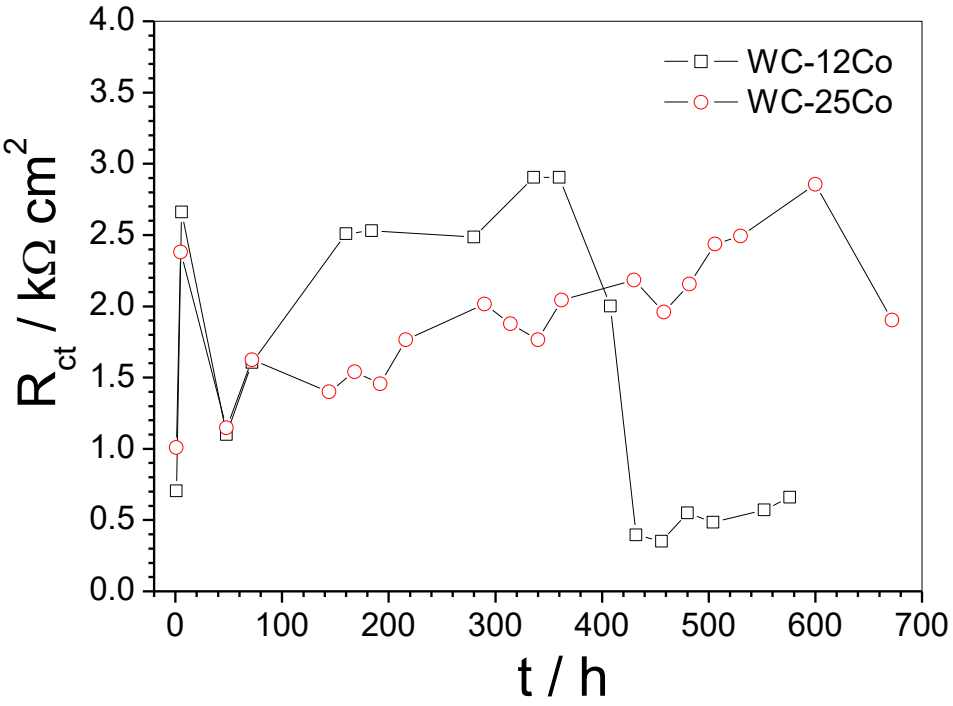

(b)

Fig. 14. (a) R_{dh} and (d) R_{ct} for WC-Co coatings in 3.5% NaCl solution at 25 ^{o}C.

This behavior can be explained considering that the electrolyte reached the substrate for WC-12Co around this immersion time (~400 h) while the coating/substrate interface remained intact for WC-25Co coating, which is also supported by cross section SEM images (Fig. 9). The lower performance of WC-12Co is also supported by its higher porosity and higher difficulty of the particles to be plastically deformed due to the lower binder content, which may generate greater quantity of defects. The R_{dh} fast increases for WC-12Co up to around 400 h of immersion and abruptly decrease to a very low value. The increase can be related to the increase of the depth of holes until to achieve a maximum value and then decreasing when the electrolyte reaches the coating/substrate interface. At this point the mechanism of dissolution is changed to consider the contribution from of Al dissolution and a

very low resistance of the corrosion products at the bottom of the holes. The resistance at the bottom of the holes is low since the hydrolysis of iron ions diminishes the local pH and the Al dissolution continues (see Fig. 9). The reduction of oxygen is practically limited to the surface of the sample.

In salt spray tests, the surface images of coatings with 500 h show no signs of substrate corrosion (Fig. 8S). However, after 1000 h small corrosion spots appear for the WC-12Co coating, while WC-25Co was apparently non-corroded at the surface. Therefore, the test was continued up to 3000 h (Fig. 8S, *SD*) and it was possible to observe a more corroded surface for WC-12Co (Fig. 8S (a), *SD*) than for WC-25Co (Fig. 8S (b), *SD*). To confirm this hypothesis, the surface of both coatings was analyzed by EDS (Fig. 9S, *SD*). Aluminum was detected on the WC-12Co surface (Fig. 9S (a), *SD*) while no Al was detected on the WC-25Co surface (Fig. 9S (b) *SD*) corroborating the better performance of this coating as indicated by all results above described. It is also interesting to note that a very simple experiment as E_{OCP} measurement (Fig. 7) could denounce the damage of the WC-12Co coating before salt spray test. Comparing the results of salt fog spray tests obtained for the WC-12Co coating prepared by HVOF [37] using conventional powder (unaltered for 130 h) and nanostructured powder (withstood 600 h), and the same coating prepared by CGS technology that showed the first signals of corrosion after 1000 h, the superiority of CGS technique is evident. The result for WC-25Co prepared by CGS was much more impressive because was practically unaltered after 3000 h of test, indicating a very high performance of this coating front the salt fog test.

4. Conclusions

The results showed that the CGS technique has a great potential to produce carbides coatings. The sprayed coatings showed well-distributed ceramic phases, no cracks, low porosity and seems to have no interconnected pores.

The WC-12Co coating is corrosion resistant at least for 400 h of immersion time in 3.5% NaCl solution. At longer immersion times in NaCl 3.5% the cobalt phase dissolution and the losing of WC particles lead to formation of interconnected porosity that allows the electrolyte access and corrosion of the substrate. The low thickness, higher porosity and probably the higher quantity of defects are responsible for weaker performance of this coating.

The compactness, low porosity, and thickness of WC-25Co coating have protected AA 7075T6 against corrosion for at least ~700 h of immersion in 3.5% NaCl solution, which was also indicated by the fact that both resistance and capacitance have maintained almost constant during the time course of the experiment. The WC-25Co coating withstood 3000 h in salt fog spray test with neutral 5 wt% NaCl at 35 °C indicating a very high performance against corrosion under these conditions.

The compressive effect of the particles by applying the CGS technology, the appropriate amount of binder and optimization of spray parameters, consequently less porous coating, are the main factors responsible for the high mechanical and anticorrosion performance of the WC-25Co coating.

5. Acknowledgements

The authors would like to thank the CNPq – Conselho Nacional de Pesquisa (Procs. 153177/2014-4 and 201325/2014-4) for the financial support and scholarships.

6. References

[1] D. Dzhurinskiy, E. Maeva, E. Leshchinsky, R. G. Maev, Corrosion protection of light alloys using low pressure cold spray, J. Therm. Spray Technol. 21 (2012) 304–313. doi:10.1007/s11666-011-9729-7.

[2] R. G. Buchheit, R. P. Grant, P.F. Hlava, B. Mckenzie, G. L. Zender, Local Dissolution Phenomena Associated with S Phase (Al[sub 2]CuMg) Particles in Aluminum Alloy 2024-T3, J. Electrochem. Soc. 144 (1997) 2621. doi:10.1149/1.1837874.

[3] A. S. El-Amoush, Intergranular corrosion behavior of the 7075-T6 aluminum alloy under different annealing conditions, Mater. Chem. Phys. 126 (2011) 607–613. doi:10.1016/j.matchemphys.2011.01.010.

[4] S. Maitra, G. C. English, Mechanism of localized corrosion of 7075 alloy plate, Metall. Trans. A. 12 (1981) 535–541. doi:10.1007/BF02648553.

[5] O. Meydanoglu, B. Jodoin, E. S. Kayali, Surface & Coatings Technology Microstructure , mechanical properties and corrosion performance of 7075 Al matrix ceramic particle reinforced composite coatings produced by the cold gas dynamic spraying process, Surf. Coat. Technol. 235 (2013) 108–116. doi:10.1016/j.surfcoat.2013.07.020.

[6] N. Birbilis, R. G. Buchheit, Electrochemical Characteristics of Intermetallic Phases in Aluminum Alloys, J. Electrochem. Soc. 152 (2005) B140. doi:10.1149/1.1869984.

[7] M. Magnani, P. H. Suegama, N. Espallargas, C. S. Fugivara, J. M. Guilemany, A. V. Benedetti, Influence of HVOF parameters on the corrosion and wear resistance of WC-Co coatings sprayed on AA7050 T7, Surf. Coat. Tech. 202 (2008) 4746–4757. doi: 10.1016/j.surfcoat.2008.04.055

[8] J. A. Picas, A. Forn, R. Rilla, E. Martin, HVOF thermal sprayed coatings on aluminium alloys and aluminium matrix composites, Surf. Coat. Technol. 200 (2005) 1178-1181. doi: 10.1016/j.surfcoat.2005.02.124

[9] S. Dosta, M. Couto, J. M. Guilemany, Cold spray deposition of a WC-25Co cermet onto Al7075-T6 and carbon steel substrates, Acta Mater. 61 (2013) 643–652. doi:10.1016/j.actamat.2012.10.011.

[10] M. Couto, S. Dosta, J. M. Guilemany, Comparison of the mechanical and electrochemical properties of WC-17 and 12Co coatings onto Al7075-T6 obtained by high velocity oxy-fuel and cold gas spraying, Surf. Coatings Technol. In press (2014) 180–189. doi:10.1016/j.surfcoat.2014.04.034.

[11] M. Couto, S. Dosta, M. Torrell, J. Fernández, J. M. Guilemany, Cold spray deposition of WC-17 and 12Co cermets onto aluminum, Surf. Coatings Technol. 235 (2013) 54–61. doi:10.1016/j.surfcoat.2013.07.011.

[12] M. Couto, S. Dosta, J. Fernandez, J. M. Guilemany. Comparison of the mechanical and electrochemical properties of WC-25Co coatings obtained by high velocity oxy-fuel and cold gas spraying. Journal of Thermal Spray Technology, v. 23, n. 8, p. 1251-1258, 2014.

[13] L. -M. Berger, Hardmetals as thermal spray coatings, Powder Metall. 50 (2007) 205–214.
doi:10.1179/174329007X246078.

[14] S. Hochstrasser(-Kurz), Y. Mueller, C. Latkoczy, S. Virtanen, P. Schmutz, Analytical characterization of the corrosion mechanisms of WC–Co by electrochemical methods and inductively coupled plasma mass spectroscopy, Corros. Sci. 49 (2007) 2002–2020.
doi:10.1016/j.corsci.2006.08.022.

[15] V. K. Champagne, The cold spray materials deposition process Fundamentals and applications, 2007, (ISBN: 9781845693787).

[16] B. H. Kear, R. K. Sadangi, M. Jain, R. Yao, Z. Kalman, G. Skandan, W. E. Mayo, Thermal Sprayed Nanostructured WC/Co Hardcoatings, J. Therm. Spray Technol. 9 (2000) 399-406.
doi: 10.1361/105996300770349863

[17] B. S. Mann, V. Arya, HVOF coating and surface treatment for enhancing droplet erosion resistance of steam turbine blades, Wear 254 (2003) 652–667.
doi: 10.1016/S0043-1648(03)00253-9

[18] T. SahraouI, N. E. Fenineche, G. Montavon, C. Coddet, Structure and wear behaviour of HVOF sprayed Cr_3C_2–NiCr and WC–Co coatings. Mater. Design 24 (2003) 309-313.
doi: 10.1016/S0261-3069(03)00059-1

[19] M. M. Lima, C. Godoy, P. J. Modenesi, J. C. Avelar-Batista, A. Davison, A. Matthews, Coating fracture toughness determined by Vickers indentation: an important parameter in cavitation erosion resistance of WC–Co thermally sprayed coatings, Surf. Coat. Technol. 177–178 (2004) 489–496.
doi: 10.1016/S0257-8972(03)00917-4

[20] B. S. Mann, V. Arya, P. Joshi, Advanced high-velocity oxygen-fuel coating and candidate materials for protecting LP steam turbine blades against droplet erosion, J. Materi. Eng. Perform. 14 (2005) 487–494.
doi: 10.1361/105994905X56188

[21] A. J. López, J. Rams, Protection of carbon steel against molten aluminum attack and high temperature corrosion using high velocity oxygen-fuel WC–Co coatings, Surf. Coat. Tech. 262 (2015) 123–133.
doi: 10.1016/j.surfcoat.2014.12.023

[22] H. Wang, X. Song, X. Wang, X. Liu, X. Wang, Fabrication of nanostructured WC–Co coating with low decarburization, Int. J. Refract. Met. H. 53 (2015) 92-97.
doi: 10.1016/j.ijrmhm.2015.05.010

[23] A. S. Praveen, J. Sarangan, S. Suresh, B. H. Channabasappa, Optimization and erosion wear response of NiCrSiB/WC–Co HVOF coating using Taguchi method, Ceram. Int. 42 (2016) 1094–1104.

doi: 10.1016/j.ceramint.2015.09.036

[24] W. Luo, U. Selvadurai, W. Tillmann, Effect of Residual Stress on the Wear Resistance of Thermal Spray Coatings, J. Therm. Spray Technol. 25 (2016) 321-330.
doi: 10.1007/s11666-015-0309-0

[25] J. Yuan, C. Ma, S. Yang, Z. Yu, H. Li, Improving the wear resistance of HVOF sprayed WC-Co coatings by adding submicron-sized WC particles at the splats' interfaces, Surf. Coat. Tech. 285 (2016) 17–23.
doi: 10.1016/j.surfcoat.2015.11.017

[26] M. Jafari, M. H. Enayati, M. Salehi, S. M. Nahvi, J. C. Han, C. G. Park, High temperature oxidation behavior of micro/nanostructuredWC-Co coatings deposited from Ni-coated powders using high velocity oxygen fuel spraying, Surf. Coat. Tech. 302 (2016) 426–437.
doi: 10.1016/j.surfcoat.2016.06.044

[27] Z. Geng, S. Hou, G. Shi, D. Duan, S. Li, Tribological behaviour at various temperatures of WC-Co coatings prepared using different thermal spraying techniques, Tribol. Int. 104 (2016) 36–44.
doi: 10.1016/j.triboint.2016.08.025

[28] T. C. Zhu, K. Yukimura, C. X. Ding, and P. Y. Zhang, Tribological Properties of Nanostructured and Conventional WC-Co Coatings Deposited by Plasma Spraying, Thin Solid Films 388 (2001) 277–282.
doi: 10.1016/S0040-6090(01)00805-7

[29] F. Ghadami, M. Heydarzadeh Sohi, S. Ghadami, Effect of TIG surface melting on structure and wear properties of air plasma-sprayed WC–Co coatings, Surf. Coat. Tech. 261 (2015) 108–113.
doi: 10.1016/j.surfcoat.2014.11.050

[30] F. Ghadami, M. Heydarzadeh Sohi, S. Ghadami, Effect of bond coat and post-heat treatment on the adhesion of air plasma sprayed WC-Co coatings, Surf. Coat. Tech. 261 (2015) 289–294.
doi: 10.1016/j.surfcoat.2014.11.016

[31] A. A. Burkov, S. A. Pyachin, Formation of WC–Co coating by a novel technique of electrospark granules deposition, Mater. Design 80 (2015) 109–115
doi: 10.1016/j.matdes.2015.05.008

[32] L. Pawlowski, The Science and Engineering of Thermal Spray Coatings, John Wiley & Sons, 2008, (ISBN: 9780471490494).

[33] V. G. Burov, I. A. Bataev, A. G. Tyurin & S. V. Veselov, Structure and properties of WC–Co coatings obtained on steel substrates by liquid state sintering in vacuum Surf. Eng. 31(2015) 540-544.
doi: 10.1179/1743294414Y.0000000415

[34] A. J. López, J. Rams, Protection of carbon steel against molten aluminum attack and high temperature corrosion using high velocity oxygen-fuel WC–Co coatings, Surf. Coat. Tech. 262 (2015) 123–133.
doi: 10.1016/j.surfcoat.2014.12.023

[35] M. S. Mahdipoor, F. Tarasi, C. Moreau, A. Dolatabadi, M. Medraj, HVOF sprayed coatings of nano-agglomerated tungsten-carbide/cobalt powders for water droplet erosion application, Wear 330-331 (2015) 338–347.
doi: 10.1016/j.wear.2015.02.034

[36] Z. Geng, S. Li, D. L. Duan, Y. Liu, Wear behaviour of WC–Co HVOF coatings at different temperatures in air and argon, Wear 330-331 (2015) 348–353.
doi: 10.1016/j.wear.2015.01.035

[37] J. M. Guilemany, S. Dosta, J. Nin, J.R. Miguel, Study of the Properties of WC-Co Nanostructured Coatings Sprayed by High-Velocity Oxyfuel, J. Therm. Spray Technol. 14 (2005) 405-413.
doi: 10.1361/105996305X59350.

[38] J. M. Guilemany, S. Dosta, J. R. Miguel, The enhancement of the properties of WC-CoHVOF coatings through the use of nanostructured and microstructured feedstock powders, Surf. Coat. Tech. 201 (2006) 1180–1190.
doi: 10.1016/j.surfcoat.2006.01.041

[39] S. Dosta, J. R. Miguel, J. M. Guilemany, Nanostructured Cermet Coatings with Enhanced properties Produced by HVOF Thermal Spray, Mater. Sci. Forum 587-588, 1024-1028.
doi:10.4028/www.scientific.net/MSF.587-588.1024

[40] M. Li, P. D. Christofides, Modeling and Control of High-Velocity Oxygen-Fuel (HVOF) Thermal Spray: A Tutorial Review, J. Therm. Spray Technol. 18 (2009) 753–768.
doi:10.1007/s11666-009-9309-2.

[41] A. Lekatou, D. Zois, D. Grimanelis, Corrosion properties of HVOF cermet coatings with bond coats in an aqueous chloride environment, Thin Solid Films. 516 (2008) 5700–5705.
doi:10.1016/j.tsf.2007.07.130.

[42] M. Magnani, P. H. Suegama, N. Espallargas, C. S. Fugivara, S. Dosta, J. M. Guilemany, a. V. Benedetti, Corrosion and Wear Studies of Cr3C2NiCr-HVOF Coatings Sprayed on AA7050 T7 Under Cooling, J. Therm. Spray Technol. 18 (2009) 353–363.
doi:10.1007/s11666-009-9305-6.

[43] Y. Wang, S. L. Jiang, Y. G. Zheng, W. Ke, W.H. Sun, J. Q. Wang, Effect of porosity sealing treatments on the corrosion resistance of high-velocity oxy-fuel (HVOF)-sprayed Fe-based amorphous metallic coatings, Surf. Coat. Tech. 206 (2011) 1307–1318.
doi:10.1016/j.surfcoat.2011.08.045.

[44] G.-C. Ji, H.-T. Wang, X. Chen, X.-B. Bai, Z.-X. Dong, F.-G. Yang, Characterization of cold-sprayed multimodal WC-12Co coating, Surf. Coat. Tech. 235 (2013) 536–543.

doi:10.1016/j.surfcoat.2013.08.021.

[45] H. J. Kim, C. H. Lee, S. Y. Hwang, Fabrication of WC-Co coatings by cold spray deposition, Surf. Coat. Technol. 191 (2005) 335–340.
doi:10.1016/j.surfcoat.2004.04.058.

[46] N. Bala, H. Singh, J. Karthikeyan, S. Prakash, Cold spray coating process for corrosion protection: a review, Surf. Eng. 30 (2014) 414–421.
doi:10.1179/1743294413Y.0000000148.

[47] S. Dosta,G. Bolelli, A. Candeli, L. Lusvarghi, I.G. Cano, J.M. Guilemany, Plastic deformation phenomena during cold spray impact of WC-Co particles onto metal substrates, Acta Mater. 124 (2017) 173–181.
doi.org/10.1016/j.actamat.2016.11.010

[48] A. Moridi, S. M. Hassani-Gangaraj, M. Guagliano, M. Dao, Cold spray coating: review of material systems and future perspectives, Surf. Eng. 30 (2014) 369–395. doi:10.1179/1743294414Y.0000000270.

[49] B. Jodoin, L. Ajdelsztajn, E. Sansoucy, A. Zúñiga, P. Richer, E. J. Lavernia, Effect of particle size, morphology, and hardness on cold gas dynamic sprayed aluminum alloy coatings, Surf. Coat. Technol. 201 (2006) 3422–3429.
doi:10.1016/j.surfcoat.2006.07.232.

[50] P. H. Gao, C. J. Li, G. J. Yang, Y. G. Li, C. X. Li, Influence of substrate hardness on deposition behavior of single porous WC-12Co particle in cold spraying, Surf. Coat. Technol. 203 (2008) 384–390.
doi:10.1016/j.surfcoat.2008.09.016.

[51] Z. Zhao, G. S. Frankel, On the first breakdown in AA7075-T6, Corros. Sci. 49 (2007) 3064–3088.

[52] Z. Zhao, G.S. Frankel, The effect of temper on the first breakdown in AA7075, Corros. Sci. 49 (2007) 3089–3111

[53] W. S. TAIT, An introduction to electrochemical corrosion testing for practicing engineers and scientists. Wisconsin Pair Odocs, 1994.

[54] K. Balani, T. Laha, A. Agarwal, J. Karthikeyan, N. Munroe, Effect of carrier gases on microstructural and electrochemical behavior of cold-sprayed 1100 aluminum coating, Surf. Coat. Technol. 195 (2005) 272–279.
doi:10.1016/j.surfcoat.2004.06.028.

[55] M. M. Sharma, T. J. Eden, B. T. Golesich, Effect of Surface Preparation on the Microstructure, Adhesion, and Tensile Properties of Cold-Sprayed Aluminum Coatings on AA2024 Substrates, J. Therm. Spray Technol. 24 (2014) 410–422.
doi:10.1007/s11666-014-0175-1.

[56] X. Zhou, P. Mohanty, Electrochemical behavior of cold sprayed hydroxyapatite/titanium composite in Hanks' solution, Electrochim. Acta. 65 (2012) 134–140.
doi:10.1016/j.electacta.2012.01.018.

[57] N. M. Melendez, A. G. McDonald, Development of WC-based metal matrix composite coatings using low-pressure cold gas dynamic spraying, Surf. Coat. Technol. 214 (2013) 101–109.
doi:10.1016/j.surfcoat.2012.11.010.

[58] K. Spencer, M. X. Zhang, Heat treatment of cold spray coatings to form protective intermetallic layers, Scr. Mater. 61 (2009) 44–47.
doi:10.1016/j.scriptamat.2009.03.002.

[59] K. Spencer, D. M. Fabijanic, M. X. Zhang, The use of Al-Al2O3 cold spray coatings to improve the surface properties of magnesium alloys, Surf. Coat. Technol. 204 (2009) 336–344.
doi:10.1016/j.surfcoat.2009.07.032.

[60] E. Zalnezhad, Ahmed A. D. Sarhan, M. Hamdi, Investigating the effects of hard anodizing parameters on surface hardness of hard anodized aerospace AL7075-T6 alloy using fuzzy logic approach for fretting fatigue application, Int. J. Adv. Manuf. Technol. 68 (2013) 453–464.
doi: 10.1007/s00170-013-4743-1

[61] B. Venkataraman, G. Sundararajan, Correlation between the characteristics of the mechanically mixed layer and wear behaviour of aluminium, Al-7075 alloy and Al-MMCs, Wear. 245 (2000) 22–38.
doi:10.1016/S0043-1648(00)00463-4.

[62] X. T. Luo, C. X. Li, F. L. Shang, G. J. Yang, Y. Y. Wang, C. J. Li, WC-Co Composite Coating Deposited by Cold Spraying of a Core-Shell-Structured WC-Co Powder, J. Therm. Spray Technol. 24 (2014) 100–107.
doi:10.1007/s11666-014-0133-y.

[63] S. Maitra, G. C. English, Mechanism of Localized Corrosion of 7075 Alloy Plate, Metall Trans. (1981) 535-541.
doi: 10.1007/BF02648553

[64] U. Tiringer, J. Kovac, I. Milosev, Effects of mechanical and chemical pre-treatments on the morphology and composition of surfaces of aluminium alloys 7075-T6 and 2024-T3, Corros. Sci. 119 (2017) 46–59.
doi: 10.1016/j.corsci.2017.02.018.

[65] S. Lameche-Djeghaba, A. Benchettara, F. Kellou, V. Ji, Electrochemical Behaviour of Pure Aluminium and Al–5%Zn Alloy in 3% NaCl Solution, Arab. J. Sci. Eng. 39 (2013) 113–122.
doi:10.1007/s13369-013-0876-7.

[66] A. B. Oliveira, A. C. Bastos, C. M. Fernandes, C. M. S. Pinho, A. M. R. Senos, E. Soares, J. Sacramento, M. L. Zheludkevich, M. G. S. Ferreira, Corrosion behaviour of WC-10% AISI 304 cemented carbides, Corros. Sci. 100 (2015) 322–331. doi:10.1016/j.corsci.2015.08.006.

[67] S. Hochstrasser-Kurz, D. Reiss, T. Suter, C. Latkoczy, D. Günther, S. Virtanen, P. J. Uggowitzer, P. Schmutz, ICP-MS, SKPFM, XPS, and Microcapillary Investigation of the Local Corrosion Mechanisms of WC–Co Hardmetal, J. Electrochem. Soc. 155 (2008) C415. doi:10.1149/1.2929822.

[68] A. M. Human, H. E. Exner, Electrochemical behaviour of tungsten-carbide hardmetals, Mater. Sci. Eng. A 209 (1996) 180–191. doi:10.1016/0921-5093(95)10137-3.

[69] Y. Liu, A. Laurino, T. Hashimoto, X. Zhou, P. Skeldon, G. E. Thompson, G. M. Scamans, C. Blanc, W. M. Rainforth, M. F. Frolish, Corrosion behaviour of mechanically polished AA7075-T6 aluminium alloy, Surf. Interface Anal. 2010, 42, 185–188. doi: 10.1002/sia.3136

[70] N. Schubert, M. Schneider, A. Michealis, The mechanism of anodic dissolution of cobalt in neutral and alkaline electrolyte at high current density, Electrochim. Acta 113 (2013) 748–754

[71] W. J. Tomlinson, C. R. Linzell, Anodic polarization and corrosion of cemented carbides with cobalt and nickel binders, J. Mater. Sci. 23 (1988) 914-918. doi:10.1007/BF01153988

[72] O. Meydanoglu, B. Jodoin, E. S. Kayali, Microstructure , mechanical properties and corrosion performance of 7075 Al matrix ceramic particle reinforced composite coatings produced by the cold gas dynamic spraying process, Surf. Coat. Technol. 235 (2013) 108–116. doi:10.1016/j.surfcoat.2013.07.020.

[73] M. E. Orazem, B. Tribollet, Electrochemical Impedance Spectroscopy, ECS-The Electrochemical Society, Pennington, NJ, 2008.

[74] W.A. Badawy, F.M. Al-Kharafi, J.R. Al-Ajmi, Electrochemical behavior of cobalt in aqueous solutions of different pH, J. Appl. Electrochem. 30 (2000) 693–704.

[75] N. M. Chavan, B. Kiran, A. Jyothirmayi, P. S. Phani, G. Sundararajan, The corrosion behavior of cold sprayed zinc coatings on mild steel substrate, J. Therm. Spray Technol. 22 (2013) 463–470. doi:10.1007/s11666-013-9893-z